materials

MDPI

Review

Advanced Non-Destructive Testing Simulation and Modeling Approaches for Fiber-Reinforced Polymer Pipes: A Review

Jan Lean Tai [1], Mohamed Thariq Hameed Sultan [1,2,3,*], Andrzej Łukaszewicz [4,*], Jerzy Józwik [5,6], Zbigniew Oksiuta [7] and Farah Syazwani Shahar [1]

1 Department of Aerospace Engineering, Faculty of Engineering, Universiti Putra Malaysia, Serdang 43400, Selangor, Malaysia; gs63398@student.upm.edu.my (J.L.T.); farahsyazwani@upm.edu.my (F.S.S.)
2 Laboratory of Biocomposite Technology, Institute of Tropical Forest and Forest Product (INTROP), Universiti Putra Malaysia, Serdang 43400, Selangor, Malaysia
3 Aerospace Malaysia Innovation Centre [944751-A], Prime Minister's Department, MIGHT Partnership Hub, Jalan Impact, Cyberjaya 63600, Selangor, Malaysia
4 Institute of Mechanical Engineering, Faculty of Mechanical Engineering, Bialystok University of Technology, Wiejska St. 45C, 15-351 Bialystok, Poland
5 Department of Production Engineering, Faculty of Mechanical Engineering, Lublin University of Technology, Nadbystrzycka St. 36, 20-618 Lublin, Poland; j.jozwik@pollub.pl
6 Institute of Technical Sciences and Aviation, The University College of Applied Sciences in Chelm, Pocztowa St. 54, 22-100 Chełm, Poland
7 Institute of Biomedical Engineering, Faculty of Mechanical Engineering, Bialystok University of Technology, Wiejska St. 45C, 15-351 Bialystok, Poland; z.oksiuta@pb.edu.pl
* Correspondence: thariq@upm.edu.my (M.T.H.S.); a.lukaszewicz@pb.edu.pl (A.Ł.)

Abstract: Fiber-reinforced polymer (FRP) pipes have emerged as a preferred alternative to conventional metallic piping systems in various industries, including chemical processing, marine, and oil and gas industries, owing to their superior corrosion resistance, high strength-to-weight ratio, and extended service life. However, ensuring the long-term reliability and structural integrity of FRP pipes presents significant challenges, primarily because of their anisotropic and heterogeneous nature, which complicates defect detection and characterization. Traditional non-destructive testing (NDT) methods, which are widely applied, often fail to address these complexities, necessitating the adoption of advanced digital techniques. This review systematically examines recent advancements in digital NDT approaches with a particular focus on their application to composite materials. Drawing from 140 peer-reviewed articles published between 2016 and 2024, this review highlights the role of numerical modeling, simulation, machine learning (ML), and deep learning (DL) in enhancing defect detection sensitivity, automating data interpretation, and supporting predictive maintenance strategies. Numerical techniques, such as the finite element method (FEM) and Monte Carlo simulations, have been shown to improve inspection reliability through virtual defect modeling and parameter optimization. Meanwhile, ML and DL algorithms demonstrate transformative capabilities in automating defect classification, segmentation, and severity assessment, significantly reducing the inspection time and human dependency. Despite these promising developments, this review identifies a critical gap in the field: the limited translation of advanced digital methods into field-deployable solutions specifically tailored for FRP piping systems. The unique structural complexities and operational demands of FRP pipes require dedicated research for the development of validated digital models, application-specific datasets, and industry-aligned evaluation protocols. This review provides strategic insights and future research directions aimed at bridging the gap and promoting the integration of digital NDT technologies into real-world FRP pipe inspection and lifecycle management frameworks.

check for updates

Academic Editor: Yuanqing Li

Received: 17 April 2025
Revised: 19 May 2025
Accepted: 22 May 2025
Published: 24 May 2025

Citation: Tai, J.L.; Sultan, M.T.H.; Łukaszewicz, A.; Józwik, J.; Oksiuta, Z.; Shahar, F.S. Advanced Non-Destructive Testing Simulation and Modeling Approaches for Fiber-Reinforced Polymer Pipes: A Review. *Materials* **2025**, *18*, 2466. https://doi.org/10.3390/ma18112466

Copyright: © 2025 by the authors. Licensee MDPI, Basel, Switzerland. This article is an open access article distributed under the terms and conditions of the Creative Commons Attribution (CC BY) license (https://creativecommons.org/licenses/by/4.0/).

Keywords: fiber-reinforced polymer (FRP); carbon fiber-reinforced polymer (CFRP); non-destructive testing (NDT); simulation; modeling; finite element method (FEM)

1. Introduction

The increasing demand for advanced materials with superior mechanical, chemical, and thermal performances has driven the widespread adoption of fiber-reinforced polymer (FRP) composites across industries such as aerospace, automotive, marine, civil infrastructure, oil and gas, and chemical processing. Among the various applications, FRP pipes have emerged as a compelling alternative to conventional metallic piping systems owing to their exceptional corrosion resistance, lightweight nature, ease of installation, and reduced lifecycle costs [1]. These attributes make FRP piping systems particularly attractive for harsh operating environments, where traditional metals are prone to corrosion, scaling, and fatigue-related failures [2–7].

Despite these advantages, FRP pipes are not immune to the defects that can arise during manufacturing, installation, and in-service operations. Such defects, including voids, delamination, fiber misalignment, and geometric deformations, can significantly compromise structural integrity and long-term reliability if left undetected [8,9]. Therefore, the implementation of robust non-destructive testing (NDT) strategies is essential to ensure quality assurance, structural health monitoring, and life-cycle management of FRP piping assets [10].

Conventional NDT methods, such as ultrasonic testing (UT), radiographic testing (RT), acoustic emission testing (AET), infrared thermography (IRT), and visual inspection (VI), have been extensively applied in various industries. However, these techniques face considerable limitations when applied to FRP materials, primarily because of their anisotropic, heterogeneous, and multilayered nature [11,12]. Complex failure modes such as delamination, fiber breakage, and matrix cracking are often difficult to detect using traditional NDT approaches, which typically rely on surface or near-surface interrogation and operator expertise. Additionally, the low density and poor contrast in radiographic imaging, limited depth resolution in thermography, and variability in human interpretation further constrain the reliability and efficiency of these conventional methods for FRP inspection [13].

Recognizing these challenges, recent research and industrial practices have increasingly turned to advanced NDT approaches that leverage digital technologies, including numerical modeling, simulation, machine learning (ML), deep learning (DL), and digital twin frameworks. These technologies offer transformative potential to enhance defect detection sensitivity, automate data interpretation, and support predictive maintenance through real-time monitoring. The finite element method (FEM), boundary element method (BEM), and Monte Carlo simulations have demonstrated significant capability in simulating defect behaviors, optimizing inspection parameters, and improving the model-assisted probability of detection (MAPOD). ML and DL algorithms have enabled the automated classification, segmentation, and severity assessment of defects across various NDT modalities [14].

Although substantial progress has been made in applying these digital techniques to general composite materials, their application to FRP piping systems, characterized by large diameters, complex geometries, and multilayered structures, remains underexplored. This highlights the urgent need for research that specifically addresses the unique challenges associated with FRP pipes, including the development of validated digital models, application-specific datasets, and standardized evaluation protocols.

This review aims to bridge this knowledge gap by systematically examining the recent advancements in digital NDT methods tailored to composite materials. Drawing on 140 peer-reviewed studies published between 2016 and 2025, this study categorized and evaluated digital NDT strategies, including numerical simulations, ML, DL, and their integration into real-time monitoring systems. The insights provided herein offer a comprehensive reference for researchers and practitioners seeking to enhance the reliability, efficiency, and cost-effectiveness of FRP pipe inspection and lifecycle management using advanced digital technologies.

2. Overview of Non-Destructive Testing (NDT)

NDT is a cornerstone of quality assurance, structural health monitoring, and life cycle management in industries such as aerospace, oil and gas, civil infrastructure, maritime, and manufacturing. NDT is defined as the process of inspecting, testing, or evaluating materials, components, or assemblies for discontinuities, defects, or differences in characteristics without permanently altering their functionality or serviceability [15–17]. Unlike destructive testing methods that require cutting, breaking, or damaging the test material, NDT enables the in situ assessment of assets throughout their service life.

2.1. Conventional NDT Techniques and Their Applications

NDT methods have been widely applied to detect surface and subsurface discontinuities in metallic structures, welds, pipelines, pressure vessels, and structural components [15]. Common conventional NDT methods include the following.

- Ultrasonic testing (UT): High-frequency sound waves are transmitted to a material to detect internal flaws, characterize thickness, or evaluate bonding quality [18–21]. UT is effective for metallic and some composite materials, but may face limitations in highly attenuative or anisotropic materials such as FRP [22].
- Radiographic testing (RT): X-rays or gamma rays are employed to capture volumetric images of internal features. While highly effective for metallic welds and castings, RT struggles with low-density materials and requires radiation safety precautions [23–26].
- Penetrant testing (PT): This involves applying a dye or fluorescent liquid to the surface of a non-porous material to reveal surface-breaking cracks or porosity after a developer is applied [27–29]. PT is limited to open-to-surface defect detection.
- Magnetic particle testing (MT): Detects surface and near-surface discontinuities in ferromagnetic materials by applying magnetic fields and ferrous particles. MT is inapplicable to nonmagnetic materials, such as FRP.
- Acoustic emission testing (AET): Transient elastic waves generated by active damage events, such as crack growth or fiber fracture under stress [30–35]. AET is suitable for real-time monitoring, but is sensitive to background noise and requires expert interpretation [36–39].
- Infrared thermography (IRT): Thermal imaging is used to detect variations in surface temperature, which may indicate subsurface defects or delamination [40–43]. Effective for near-surface defects, but limited by depth resolution.
- Visual inspection (VI): The simplest form of NDT that relies on direct observation to detect visible defects. However, it is inherently limited to surface-level defects and is highly subjective.

2.2. Challenges of Conventional NDT on Composite Structures

Although these methods are well-established for metallic materials, their application in FRP composites, particularly FRP piping systems, presents significant challenges.

- Anisotropic and heterogeneous nature: FRP materials consist of fiber and resin matrices with directional properties, making wave propagation unpredictable in UT and other wave-based methods.
- Complex defect modes: FRP structures exhibit unique failure mechanisms, such as delamination, fiber breakage, matrix cracking, and void formation, many of which are difficult to detect using surface-focused methods such as PT or VI.
- Low density and low contrast: RT struggles to differentiate between the matrix and fiber in FRP materials owing to the low X-ray absorption contrast compared to metallic materials.
- Human interpretation dependency: Many NDT results, especially from AET and UT, rely heavily on the expertise of the inspector, leading to inconsistencies and subjectivity in defect characterization [44].
- Limited depth resolution: Techniques such as IRT and PT are constrained to detect surface or near-surface anomalies, which may not capture the critical subsurface damage in thick-walled FRP structures.
- Inspection time and cost: Traditional methods may require multiple setups, manual scanning, and subjective interpretation, leading to increased inspection times and costs, particularly for large or complex FRP installations.

2.3. The Need for Advanced NDT Approaches

To overcome these limitations, the industry is shifting toward advanced NDT, which integrates digital technologies, computational modeling, and data-driven algorithms to enhance defect-detection sensitivity, automate data interpretation, and improve inspection reliability. This includes the following:

- Numerical simulation and modeling (e.g., FEM and BEM): this allows for the prediction and visualization of defect interactions with inspection signals before physical testing [45–48].
- ML and DL: automated feature extraction, defect classification, and severity assessment using large datasets of inspection signals or images [49–53].
- Digital twin and real-time monitoring: this enables continuous asset health monitoring through virtual replicas of physical systems, integrating sensor data for predictive maintenance [54–57].
- MAPOD: quantifying inspection reliability through combined experimental and simulation-based probability of detection (POD) studies, reducing dependence on costly physical trials [58–60].
- Advanced imaging and sensing technologies: such as X-ray computed tomography (XCT) [61–64], phased array ultrasonic testing (PAUT) [65–69], eddy current testing (ECT) [70–72], high-frequency eddy current testing (HF-ECT) [73–75], and thermographic methods optimized through simulation [76–78].

These approaches offer significant benefits, including enhanced defect sensitivity and resolution, for detecting microdefects or complex damage modes. They also improve automation and consistency in defect evaluation, effectively reducing human bias and variability. Additionally, the optimized inspection parameters derived from the simulation contribute to reducing both inspection time and associated costs. Finally, these methods facilitate integration with predictive maintenance frameworks, condition-based monitoring (CBM), and comprehensive lifecycle management [79].

3. Fiber-Reinforced Polymer/Plastic

FRP is a composite material composed primarily of fibers and resins. This versatile material has numerous synonymous and dissimilar appellations that can cause perplexity

among individuals. FRPs are manufactured by embedding fibers into a polymer matrix. This material surpasses traditional materials in several applications. To provide a more comprehensive understanding of FRPs, the following section provides an overview of the various available types of FRP.

3.1. Types of Fiber-Reinforced Polymer

FRP materials are a versatile group of composites specifically designed for particular applications and engineering requirements. The selection of the reinforcement fibers and polymer matrix plays a critical role in determining the characteristics of the material. The following are some fundamental types of FRP, and Table 1 provides a detailed overview.

Table 1. Type of FRP overview.

FRP Composite Type	Reinforcement	Key Properties	Typical Applications	Typical Mechanical Properties
GFRP (Glass Fiber-Reinforced Polymer)	Glass fibers	High strength, corrosion resistance, electrical insulation	Construction, automotive, marine	Tensile Strength: 500–900 MPa, Modulus: 35–55 GPa, Density: 1.8–2.0 g/cm^3
CFRP (Carbon Fiber-Reinforced Polymer)	Carbon fibers	High strength-to-weight ratio, high stiffness, corrosion resistance	Aerospace, automotive, sporting goods, structural engineering	Tensile Strength: 600–3500 MPa, Modulus: 70–250 GPa, Density: 1.5–1.6 g/cm^3
AFRP (Aramid Fiber-Reinforced Polymer)	Aramid fibers (e.g., Kevlar)	High tensile strength, impact resistance, flame resistance	Body armor, protective gear, structural applications	Tensile Strength: 3000–3600 MPa, Modulus: 60–125 GPa, Density: 1.44 g/cm^3
BFRP (Basalt Fiber-Reinforced Polymer)	Basalt fibers	High-temperature resistance	Construction, infrastructure repair and reinforcement	Tensile Strength: 2000–4840 MPa, Modulus: 89–93 GPa, Density: 2.7 g/cm^3
NFRP (Natural Fiber-Reinforced Polymer)	Natural fibers (e.g., jute, hemp, flax)	Environmental friendliness, low density, flexibility, cost-effectiveness	Automotive interiors, furniture, construction	Tensile Strength: 200–900 MPa, Modulus: 10–30 GPa, Density: 1.2–1.5 g/cm^3
HFRP (Hybrid Fiber-Reinforced Polymer)	Combination of various fiber types	Balanced properties (strength, stiffness, cost-effectiveness)	Wide range of applications	Varies based on fiber combination

1. Glass fiber-reinforced polymer (GFRP): GFRP composites utilize glass fibers as reinforcement. These materials are used in applications requiring high strength, corrosion resistance, and electrical insulation and are prevalent in the construction, automotive, and marine industries [80–82].
2. Carbon fiber-reinforced polymer (CFRP): CFRP composites employ carbon fibers as reinforcements with a noteworthy strength-to-weight ratio and stiffness. Apart from typical carbon material attributes such as high-temperature resistance, friction resistance, and corrosion resistance, CFRP possesses exceptional specific strength, specific modulus, and fatigue resistance [83,84]. CFRPs can be used as CFRP materials in aerospace, automotive, sporting goods, and structural engineering applications [85].
3. Aramid fiber-reinforced polymer (AFRP): AFRP composites incorporate aramid fibers, such as Kevlar, for reinforcement. These fibers impart high tensile strength, impact resistance, and flame resistance to the composite materials [86]. AFRP is commonly used in body armor, protective gears, and structural applications where high strength and durability are critical [87,88].

4. Basalt fiber-reinforced polymer (BFRP): BFRP composites that use basalt fibers for reinforcement are highly effective for high-temperature applications and are commonly used in the repair and reinforcement of infrastructure in the construction industry [89–92].
5. Natural fiber-reinforced polymer (NFRP): NFRP composites incorporate natural fibers, such as jute, hemp, or flax, as reinforcements and are valued for their environmental friendliness, nonhomogeneous composition, and diverse applications in automotive interiors, furniture, and construction [93–95]. Natural fibers have gained significant attention in recent years owing to their numerous advantages including cost-effectiveness, low density, exceptional flexibility, recyclability, and sustainability. However, their widespread use is limited by their relatively low impact strength and hydrophilicity [96].
6. Hybrid fiber-reinforced polymer (HFRP): HFRP composites are formulated by combining various fiber types, including natural/synthetic hybrid fibers, to achieve a comprehensive balance of properties such as strength, stiffness, and cost-effectiveness [97–99]. These composites were designed to satisfy the specific requirements of applications that require a combination of attributes [100–103].

CFRP and GFRP are widely used in the industry owing to their respective advantages, and GFRP is also referred to as GRP. Additionally, reinforced thermosetting resin plastic (RTR) has been used by some researchers because of the use of thermosetting resins. The term "resin" refers to a type of thermosetting plastic used to reinforce fiberglass. As shown in Figure 1, three primary types of thermosetting resins are used in the production of GRP: polyester, epoxy, and vinyl ester [104]. The use of different resins results in the production of three distinct GRP sub-types: glass fiber-reinforced epoxy (GRE) [105–107], glass fiber-reinforced vinyl ester (GRVE) [108–111], and glass fiber-reinforced polyester (GRUP) [112]. Table 2 summarizes the three main types of resin used in FRP manufacturing, highlighting their advantages, disadvantages, and typical mechanical properties for easier comparison [113–115].

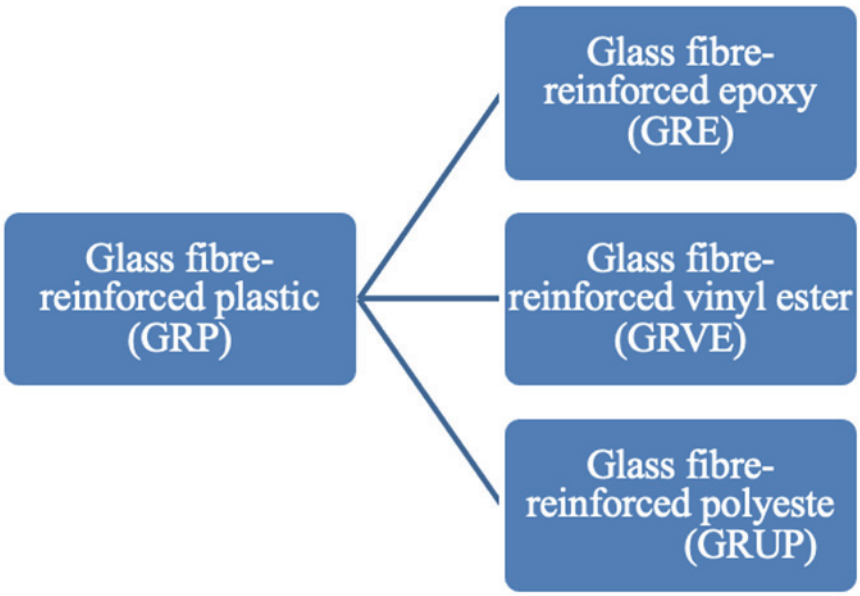


Figure 1. Various types of glass-fiber reinforced plastic.

Table 2. Summary of resin types, advantages, disadvantages, and typical properties for FRP manufacturing.

Resin Type	Advantages	Disadvantages	Typical Properties
Polyester	Low cost, good chemical resistance, easy to process	Lower mechanical strength, poor elongation	Tensile Strength: 40–100 MPa, Tg: 70–80 °C, Low viscosity
Epoxy	High strength, excellent adhesion, good mechanical properties	Higher cost, sensitive to curing conditions	Tensile Strength: 70–150 MPa, Tg: 120–180 °C, Moderate viscosity
Vinyl Ester	High chemical resistance, good mechanical properties, good toughness	More expensive than polyester, handling precautions required	Tensile Strength: 80–130 MPa, Tg: 90–140 °C, Moderate viscosity

Thermoplastic Resins in FRP Manufacturing

Although thermosetting resins, such as polyester, vinyl ester, and epoxy, have long been dominant in FRP manufacturing because of their excellent mechanical and thermal properties after curing, thermoplastic resins are gaining increasing attention as viable alternatives [116,117]. This shift is particularly notable in applications requiring recyclability, improved impact resistance, and thermoformability [118]. Unlike thermosets, thermoplastic resins do not undergo irreversible chemical crosslinking during processing. Instead, they can be softened and reshaped by heating, making them suitable for fusion bonding, recycling, and thermoforming processes. This property significantly enhances processing flexibility and end-of-life sustainability.

The common thermoplastic resins used in FRP applications include polypropylene (PP) [119–123], polyethylene terephthalate (PET) [124–128], polyether-ether-ketone (PEEK) [129–132], and polyamide (PA or Nylon) [133–135]. These resins offer several advantages, such as high impact resistance, good chemical and moisture resistance, thermal reprocessability, and recyclability. However, they also have limitations, including higher processing temperatures, equipment costs, and lower thermal stability than high-performance thermosets.

In the context of FRP pipe manufacturing, thermoplastic matrix composites have been explored for various applications, including chemical processing pipelines, oil and gas transportation lines, and water and wastewater infrastructure [136]. Emerging manufacturing methods, such as thermoplastic filament winding and fusion bonding, further enhance the industrial viability of thermoplastic-based FRP pipes. These methods enable the production of lightweight, corrosion-resistant, and recyclable piping systems that are suitable for a wide range of industrial applications. Table 3 provides a comparative summary of commonly used thermoplastic resins, highlighting their key properties, advantages, limitations, and typical applications to assist in the material selection for specific FRP manufacturing requirements.

Table 3. Summary of common thermoplastic resins used in FRP manufacturing: key properties, advantages, limitations, and applications.

Thermoplastic Resin	Key Properties	Advantages	Limitations	Example Applications
Polypropylene (PP)	Low density, good chemical resistance	Lightweight, cost-effective, corrosion-resistant	Low thermal stability, limited mechanical strength	Chemical pipelines, water systems
Polyethylene Terephthalate (PET)	Good mechanical strength, chemical resistance, recyclable	High impact resistance, good environmental profile	Moisture sensitivity, thermal limitations	Water treatment, automotive parts
Polyetheretherketone (PEEK)	High mechanical and thermal performance	Excellent chemical and thermal resistance, high strength-to-weight	High cost, requires high processing temperature	Aerospace, oil and gas piping
Polyamide (Nylon)	High toughness, moderate moisture absorption	Good impact resistance, flexible processing	Moisture sensitivity, lower chemical resistance than PEEK	Automotive, industrial piping

3.2. Manufacturing Method

Understanding the various FRP classifications is crucial, as it paves the way for in-depth knowledge of the manufacturing processes involved in the production of FRP materials. The manufacturing of FRP materials encompasses a range of manufacturing processes, each of which is tailored to a specific product type and characteristics. The four commonly employed manufacturing methods are as follows.

1. Pultrusion process: Pultruded FRP composites are fabricated by pulling continuous fibers through a resin bath and then through a shaping die. This process created continuous profiles with consistent cross-sectional shapes. Pultruded FRP is used in structural applications, such as beams, tubes, and rods [137].
2. Filament-wound process: Filament-wound FRP composites are created by winding continuous fibers, typically glass or carbon, around a rotating mandrel and impregnating them with resin. This method produces cylindrical or tubular shapes and is commonly used in pressure vessels and pipes [138].
3. Hand lay-up process: Hand lay-up FRP involves manually applying layers of fiber and resin to a mold. This is a versatile method for creating custom FRP products or for small-area repair of FRP products. However, they may exhibit variations in their quality and consistency [139].
4. Spray-up process: Spray-up FRP involves spraying a mixture of chopped fibers and resin onto a mold. This is a fast and cost-effective method to obtain large and simple shapes [140].

Filament wounds or filament windings are typically used for large-diameter pipes and can be efficiently produced through continuous winding. However, pultrusion is more suitable for smaller and singular designs such as tubes, L-channels, and C-channels. The efficiency of the hand lay-up process is limited because it is purely handmade, whereas the spray-up process has the potential to increase productivity. Figure 2 shows the schematic of the aforementioned processes.

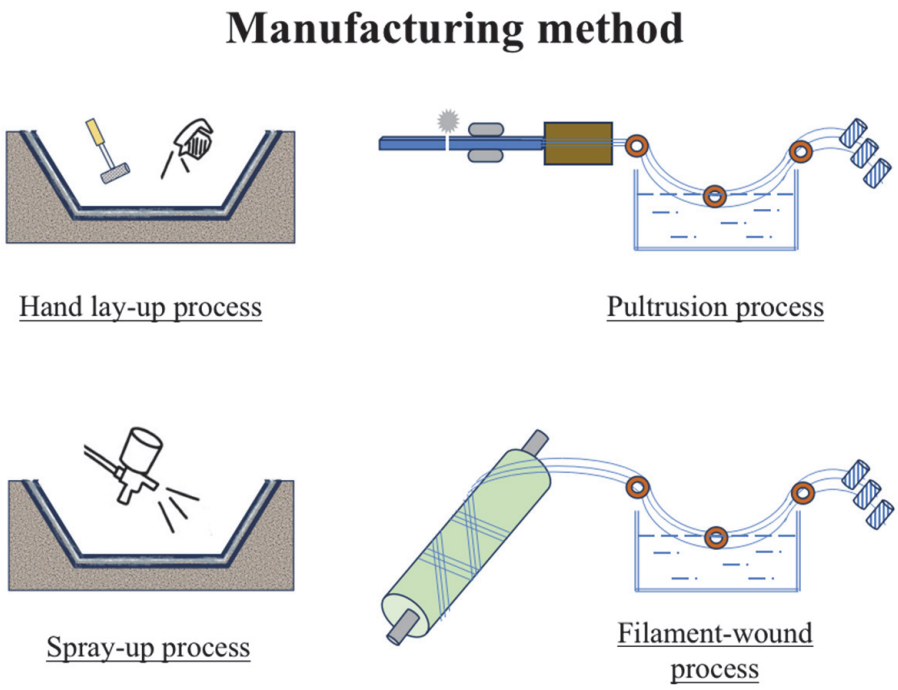


Figure 2. Schematic of FRP manufacturing methods.

3.2.1. Vacuum- and Pressure-Assisted Resin Infusion Methods

Vacuum-assisted resin infusion (VARI) or vacuum-assisted resin transfer molding (VARTM) is used to produce large-scale composite structures, including FRP pipes. This process involves placing dry fiber reinforcements into a mold and using vacuum pressure to infuse the resin through the fiber network, ensuring complete wetting and minimizing void content [141–143].

The process begins by laying dry fibers into a mold, which is then sealed in a vacuum bag. A vacuum pump was used to evacuate the air from the mold and create a pressure differential. This pressure difference draws the liquid resin into the mold through the inlet ports, allowing it to saturate the fiber layers under controlled pressure [144]. Once the resin has fully infiltrated the fibers and the curing process is complete, the part is demolded, resulting in a high-quality, void-free composite structure [145,146].

This method has several advantages. This enables a high fiber-to-resin ratio, which significantly improves the mechanical properties of the composite. Compared with hand lay-up and other open-mold methods, VARI/VARTM results in reduced void content. This leads to an enhanced structural integrity and performance of the final product [147]. Additionally, this technique is associated with lower labor costs and is highly scalable for the production of large or complex parts [148,149]. From an environmental perspective, it minimizes resin waste and reduces operator exposure to volatile organic compounds (VOCs).

However, there are some limitations to the study. The process requires specialized tooling and equipment, which may involve significant initial investments. Process control is critical to ensure complete impregnation of the fibers and avoid issues such as resin starvation. Currently, this method is primarily limited to thermosetting resins, although research and development are ongoing to extend this technique to thermoplastic resins.

In FRP pipe manufacturing, vacuum- and pressure-assisted resin infusion methods are particularly valuable. They are commonly used for the production of large-diameter FRP pipes, pipe fittings, and custom pipe sections, which require high mechanical performance and dimensional stability. Industries such as marine, chemical, and oil and gas industries benefit significantly from this technology [150,151]. These sectors require materials with excellent corrosion resistance and mechanical strength, both of which are characteristics

of FRP pipes manufactured using VARI/VARTM. By incorporating vacuum- or pressure-assisted resin infusion methods, manufacturers can achieve superior structural performance and quality control, making this technique increasingly popular for use in high-specification FRP piping systems [152].

By incorporating vacuum- or pressure-assisted resin infusion methods, manufacturers can achieve superior structural performance and quality control, making this technique increasingly popular for high-specification FRP piping systems.

Figure 3 illustrates the schematic layout of the VARI process, highlighting the flow of the resin from the inlet reservoir to the fiber reinforcement under vacuum pressure. The use of a sealed vacuum bag and controlled resin flow ensured the complete impregnation of the fiber layers, resulting in a high-quality, void-free composite. This process not only optimizes the mechanical performance, but also reduces material waste, making it an attractive option for scalable and sustainable FRP pipe production [152].

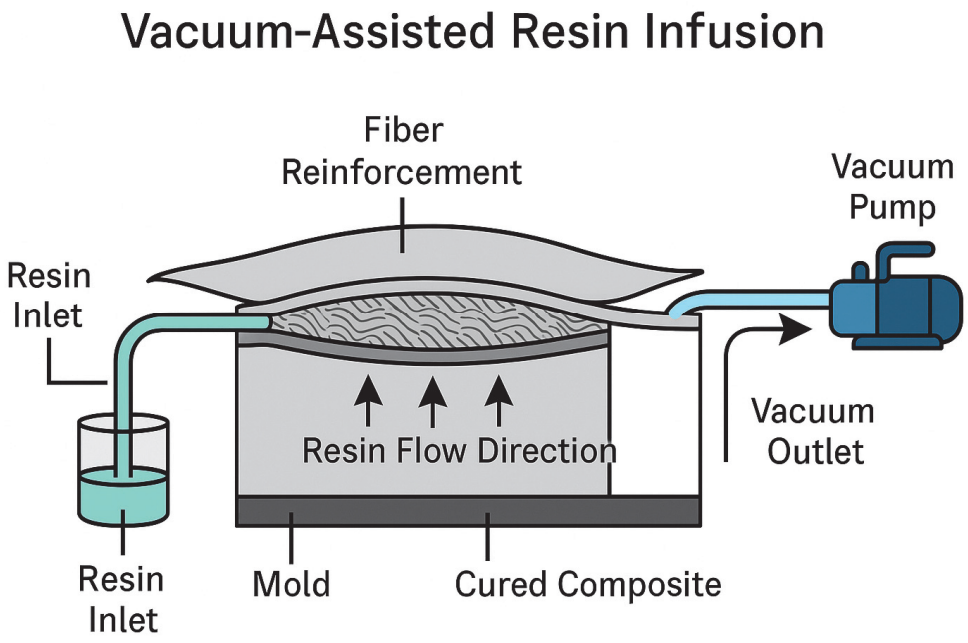


Figure 3. Schematic representation of vacuum-assisted resin infusion process for FRP manufacturing.

3.2.2. Materials and Manufacturing Technologies for FRP Pipe Production

FRP pipes typically consist of a composite laminate structure composed of various materials, including reinforcement fibers, matrix resins, fillers, and additives. Reinforcement fibers play a crucial role in the strength and stiffness of composites. Glass fibers, such as E-glass and S-glass, are the most common owing to their cost-effectiveness, corrosion resistance, and high tensile strength [153]. Carbon fibers are used for high-pressure or high-stiffness applications, offering superior strength-to-weight ratios. Aramid fibers such as Kevlar are applied in impact-resistant or ballistic protection scenarios [154].

Matrix resins serve as binding agents in the composites. Thermosetting resins, including polyester, vinyl ester, and epoxy resins, such as GRE, GRVE, and GRUP, are widely used because of their excellent mechanical and thermal properties after curing. Thermoplastic resins such as polypropylene, PEEK, and PET are gaining attention for their recyclability, improved impact resistance, and thermoformability [155].

Fillers and additives, such as silica, alumina trihydrate, and fire retardants, may be incorporated to enhance the thermal, chemical, and flame resistance of the composite.

Several manufacturing technologies have been employed in the production of FRP pipes, each offering different performance characteristics and cost implications [156]. Fila-

ment winding involves winding continuous fibers under tension over a rotating mandrel in precise patterns such as hoop, helical, or polar. This method is suitable for high-pressure pipes with consistent fiber alignment and can be automated for large-scale production. Centrifugal casting, or spinning, involves placing resin and fibers in a rotating mold to create a dense, smooth inner surface. This method is commonly used for sewage treatment, drainage, and low-pressure applications. Pultrusion involves pulling continuous fibers through a resin bath and heated die to produce constant cross-sectional profiles, such as pipe supports or structural members. Hand lay-up and spray-up involve manually applying fibers and resin to a mold or form, making them suitable for custom or low-volume production, although they offer lower consistency than automated methods. VARI/VARTM provides high-quality void-free laminates for large-diameter or high-specification pipes. Fusion bonding for thermoplastic pipes involves heat-fusing thermoplastic layers to form chemically resistant, recyclable piping systems.

These diverse materials and manufacturing technologies allow the production of FRP pipes that are tailored to meet specific performance requirements and application demands [157].

3.3. Common Defects in FRP Materials During Manufacturing

Although FRP materials offer several advantages, they are not immune to defects during manufacturing. Identifying and addressing defects is crucial for ensuring product integrity. Common defects include the following:

1. Voids: Voids are areas within composite materials that contain air pockets that weaken their structure and reduce their strength [158]. The formation of voids can be attributed to several factors including incomplete resin wetting, entrapped air bubbles during lay-up or infusion, and resin shrinkage. To prevent the formation of voids, it is crucial to ensure thorough mixing of the resin and proper wetting of the fibers [159]. Additionally, vacuum- or pressure-assisted resin infusion should be implemented to reduce air entrapment, and the curing conditions should be controlled to minimize resin shrinkage [160].
2. Delamination: Delamination is a phenomenon that occurs when the layers of reinforcement fibers separate, leading to a reduction in the material's integrity and expansion during service while increasing the stress and impact [161]. The formation of delamination can be attributed to several factors, including poor bonding, inadequate pressure during curing, and repeated thermal stress. To prevent delamination, it is crucial to ensure that adequate pressure is applied during curing and good surface preparation. Additionally, the design components should be minimized to reduce the thermal cycling stress and prevent delamination [162–164].
3. Fiber misalignment: Improper fiber alignment can result in the creation of weak points or anisotropy in the composite material. This may be caused by inadequate equipment maintenance, incorrect positioning during the lay-up process, or inadequate training of personnel. Regular equipment maintenance and personnel training are essential for preventing fiber misalignment [165,166].
4. Resin-rich or resin-poor areas: An inconsistent distribution of resin or uneven fiber distribution can result in areas with either excessive or inadequate resin content, which can negatively impact the structural integrity [158]. This is caused by improper resin application during the lay-up process, and the resin flow within the mold may not be consistent. To prevent the need for careful control of resin application, it is vital to ensure even coverage and consistent resin flow.
5. Surface imperfections: The presence of cracks, bubbles, or other irregularities on the surfaces of FRP components can negatively affect their aesthetic appearance and

functionality. The appearance of these imperfections can be attributed to several factors, including defects or damage to the mold, contaminants, or foreign particles present during the lay-up process, and variations in the curing process. To prevent the formation of surface imperfections, it is recommended to regularly inspect and maintain the molds, ensure a clean and controlled environment during the lay-up process, and monitor and control curing conditions to ensure consistency.

Gaining insight into the underlying causes of these defects is of paramount importance to proactively address them during the manufacturing process. It is worth noting that additional defects can manifest when FRP materials are in service, depending on the particular environment and service, such as joint defects, matrix cracks, and fiber breaks.

Geometric Deformation Defects

In addition to internal defects, such as voids, porosity, and delamination, geometric deformation defects pose significant challenges in the manufacture of FRP pipes and composite components. These defects include spring-in, warpage, and shrinkage, which can compromise the dimensional accuracy, fit-up, and long-term mechanical performance of the final product, respectively.

1. Spring-in: Spring-in manifests as an angular deviation in the curved or angled parts when they relax after demolding. This defect is commonly observed in elbows, flanges, and pipe fittings, where the final angle exceeds the intended dimensions, leading to assembly and alignment complications. The root causes of spring-in include residual stresses within the composite, differential thermal contraction between the fiber and resin matrix, and uneven curing shrinkage. To mitigate spring-in, manufacturers can optimize tooling design and cure schedules, implement symmetric fiber layups to balance stresses, and utilize process simulations to predict and compensate for the expected deformations. Additionally, post-curing treatments or mechanical trimming can be employed to restore dimensional tolerances [167].
2. Warpage: Warpage occurs when a component is distorted out of the plane, resulting in dimensional instability or surface waviness. In FRP pipes, warpage can affect the roundness, straightness, and flange flatness of the product, thereby complicating sealing and joint integrity. The factors contributing to warpage include asymmetric layups, uneven curing, thermal gradients, and tooling design limitations [168]. To prevent warpage, it is essential to design symmetric fiber layups, control curing conditions to ensure uniformity, and optimize tooling to minimize the thermal gradients. Advanced process simulations can also be used to predict and compensate for warpage tendencies, while post-processing steps, such as controlled cooling and mechanical straightening, can help restore dimensional accuracy [169,170].
3. Shrinkage: Shrinkage is another critical geometric deformation defect that occurs during the curing or cooling of FRP components. As the resin cures and cools, it contracts, potentially leading to dimensional reductions in pipe diameter or thickness [171]. Excessive shrinkage can cause fitment issues and compromise the pressure containment capability of the pipes. The primary causes of shrinkage include the inherent volumetric contraction of the resin during curing and the differential cooling rates between the composite and mold [172,173]. To mitigate shrinkage, manufacturers can select low-shrinkage resin formulations, optimize curing cycles to control cooling rates, and employ shrinkage-compensating tooling designs. Additionally, incorporating reinforcing fibers with appropriate coefficients of thermal expansion can help reduce shrinkage-related deformation [174,175].

Recognizing and mitigating these geometric deformation defects is essential to ensure that FRP piping systems satisfy stringent dimensional and performance requirements, particularly in critical infrastructure and industrial applications.

4. Using Digital Technologies to Enhance NDT Performance

In the rapidly evolving world of technology, NDT has transitioned from traditional inspection methods to more sophisticated techniques that harness various technologies to achieve faster and more accurate detection. A comprehensive literature review shows that these technologies can be broadly categorized into numerical modeling, simulation, ML, and DL. Some researchers have combined these approaches to enhance NDT performance.

This section aims to showcase specific success case studies that highlight the application of numerical modeling, simulation, ML, DL, or a combination of these approaches in various NDT methods for composites or other materials. The practical benefits and advantages of these digital technologies in the field of NDT can be obtained by examining these success stories.

4.1. Numerical Modeling and Simulation: Purpose and Classification of Methods

As the complexity of FRP materials and their structural applications continues to grow, the limitations of traditional NDT methods, such as operator dependency, limited depth resolution, and insufficient sensitivity to composite-specific defects, have become increasingly apparent. To address these challenges, numerical modeling and simulation have emerged as essential tools for enhancing NDT performance by providing predictive insights, optimizing inspection parameters, and reducing reliance on costly experimental trials.

The purpose of this section is threefold.

1. To categorize the leading numerical methods applied in NDT, including FEM, BEM, finite integration technique (FIT), Monte Carlo simulation, and semi-analytical models.
2. To demonstrate their practical applications across various NDT techniques, they were supported by findings from recent literature.
3. To summarize their comparative advantages, limitations, and reported performance metrics to assist practitioners and researchers in selecting appropriate methods for specific NDT scenarios.

The following subsections group the literature by modeling methodology and highlight their impact on the advancement of NDT capabilities for composite materials, particularly FRP structures.

4.1.1. Finite Element Method Applications in NDT

The FEM is among the most widely applied numerical modeling techniques in advanced NDT research. Its ability to handle complex geometries, multiphysics interactions, and material anisotropy makes it particularly suited for studying wave propagation, stress analysis, and thermal behavior in FRP materials [176–178].

The FEM discretizes a complex structure into smaller elements, allowing researchers to simulate how ultrasonic waves, thermal energy, or mechanical stresses interact with defects such as delamination, voids, or cracks. Multiple studies have successfully employed the FEM to enhance the predictive capability and reliability of various NDT techniques.

- Acharjee and Bandyopadhyay [179] applied FEM to assess the structural integrity of fire-damaged reinforced concrete members, demonstrating how temperature load impacts structural responses and validating their computational predictions with experimental results.
- Munalli et al. [180] combined FIT and FEM to simulate microwave-based NDT to detect damage in CFRP materials. Their study analyzed scattering parameters (S-parameters)

to differentiate between healthy and damaged regions, showing a good correlation with experimental data.

- Evans et al. [181] integrated the FEM with experimental validation to predict the type, location, and extent of impact damage in CFRP laminates subjected to low-velocity impacts. Their hybrid modeling-experimental approach provided a comprehensive understanding of the damage mechanisms.
- Feito et al. [182] used FEM to simulate the mechanical behavior of open-hole CFRP laminates under tensile and fatigue loading and achieved close agreement with the experimental strain distribution and crack progression results.
- Fang and Maldague [40] utilized the FEM to model the thermal response of CFRP specimens with controlled defects. Their simulation data were subsequently used to train a gated recurrent unit (GRU) deep learning model, which successfully quantified the defect depth from thermal signals.
- Ratsakou et al. [183] validated a semi-analytical truncated region eigenfunction expansion (TREE) model by comparing it with FEM-based COMSOL simulations for the IRT of delaminated planar structures, confirming FEM's role as a validation benchmark.
- Notebaert et al. [184] demonstrated the use of COMSOL Multiphysics FEM simulations to model the active thermographic inspections of additively manufactured composite parts, achieving a high degree of agreement between the simulated and experimental results.
- Kim et al. [185] focused on modeling and simulating IRT to detect subsurface defects in hydroelectric penstocks. The study used ANSYS version 19.2.0 to build a 3D penstock model and simulate lock-in infrared thermography.

These studies illustrate the versatility and robustness of the FEM in simulating a wide range of NDT scenarios, from ultrasonic wave propagation to thermal and mechanical analyses. Despite its computational demands, the FEM remains a powerful tool for predicting defect responses, optimizing inspection parameters, and enhancing the reliability of NDT for FRP materials.

4.1.2. Boundary Element Method (BEM) and Semi-Analytical Models

Although FEM is well established for simulating multi-physics and complex geometries, its computational cost can be prohibitive, particularly for large-scale or frequency-domain simulations. The BEM and semi-analytical models offer computationally efficient alternatives for specific NDT applications, particularly in electromagnetic and wave-based inspections [186,187].

BEM focuses on discretizing only the boundary of the geometry rather than the entire volume, significantly reducing the computational resources for problems involving infinite or semi-infinite domains, such as electromagnetic field simulations. The BEM has shown a particular value in ECT and POD modeling [188].

- Baskaran et al. [189] developed a BEM-based framework to model the eddy current responses for flaw detection in conductive materials. Their study integrated BEM results with Gaussian statistical models to improve POD estimation, demonstrating that BEM could accurately compute impedance changes with less than 5% error compared to the experimental data.
- Apostol et al. [72] proposed analytical and numerical models based on Maxwell's equations to enhance ECT signal interpretation. Their approach validated the numerical results using semi-analytical solutions, reinforcing the reliability of the BEM in electromagnetic NDT.
- Hachi et al. [190] employed a hybrid 3D FEM and magnetic vector potential formulation to simulate the eddy current density distribution in CFRP composites. Their

work highlighted the anisotropic electrical behavior of CFRP, demonstrating BEM's applicability in complex material characterizations.

Semi-analytical models, such as eigenfunction expansions and heat diffusion equations, provide rapid approximate solutions for thermal, ultrasonic, and electromagnetic phenomena [191]. Although less flexible than numerical methods for complex geometries, they offer significant computational speed for specific controlled scenarios.

- Ratsakou et al. [183] developed a TREE semi-analytical model to simulate heat propagation in delaminated structures. Their results showed strong agreement with the FEM-based COMSOL simulations, validating the efficiency and accuracy of their approach for infrared thermography applications.
- Apostol et al. [72] further demonstrated the usefulness of analytical modeling in eddy current analysis, providing closed-form solutions for magnetic vector potentials in layered media.
- Hachi et al. [190] validated their numerical results using analytical solutions for unidirectional CFRP plates, ensuring the consistency and reliability of their computational models.

Although BEM and semi-analytical methods may not match FEM's versatility for highly detailed or nonlinear problems, they offer computational advantages for specialized applications, particularly when combined with POD modeling or signal interpretation frameworks. Their validation through comparison with FEM or experimental data enhanced the confidence in their predictive capabilities.

4.1.3. Finite Integration Technique (FIT), Monte Carlo Methods, and Other Numerical Approaches

Finite Integration Technique

FIT has gained traction as a computational method particularly suited for high-frequency electromagnetic simulations such as microwave and millimeter-wave NDT. FIT discretizes Maxwell's equations in integral form, making it well-suited for analyzing the interaction of electromagnetic waves with complex materials.

- Munalli et al. [180] combined FIT and FEM to simulate the use of microwave NDT techniques for damage detection in CFRP. Their study demonstrated that variations in S-parameters could effectively distinguish between healthy and defective areas. FIT simulations correlated well with experimental measurements, confirming their value for electromagnetic wave-based NDT applications.

Monte Carlo Simulation Methods

Monte Carlo methods are statistical simulation techniques that model the probabilistic behavior of complex systems through repeated random sampling [192,193]. These methods are particularly valuable in radiographic NDT, where they simulate X-ray and gamma-ray interactions with materials to optimize imaging parameters and reduce safety risks [194].

- Mousa et al. [195] used the GEANT4 GATE toolkit to simulate computed radiography testing (CRT) of carbon steel plates and pipes, demonstrating improved image quality and system optimization without the need for extensive physical trials.
- Sari et al. [196] applied Monte Carlo simulations to model gamma-ray backscatter for detecting voids in concrete, validating the method using experimental data to ensure accurate calibration.
- Kumar et al. [197] optimized the radiographic parameters for inspecting nuclear fuel reprocessing tanks using aRTist, a radiography simulation software, and achieved good alignment with experimental observations.

Other Numerical Techniques and Hybrid Approaches

Several other specialized numerical tools and hybrid approaches have also been reported in the literature, expanding the range of simulation techniques applicable to advanced NDT.

- Osipov et al. [198] introduced a high-performance algorithm for simulating digital radiography testing (DRT) of large, complex industrial components, enabling realistic image generation without extensive experimental testing.
- Rodat et al. [199] presented a metamodeling simulator that integrates human factors into MAPOD studies, allowing a realistic simulation of human-influenced inspection outcomes.
- Lei et al. [200] used SimSUNDT software for a fully simulation-based POD study of PAUT, demonstrating the feasibility of generating reliable POD curves without extensive physical experiments.

These alternative methods highlight the breadth of simulation capabilities available to researchers and practitioners in NDT. Although each technique has its specific strengths and limitations, their combined use in hybrid modeling frameworks often yields more robust, cost-effective, and accurate NDT solutions, as summarized in Table 4.

Table 4. Comparative summary of numerical modeling methods.

Modeling Method	Strengths	Limitations	Typical Applications	Reported Performance
Finite Element Method (FEM)	Handles complex geometries, multi-physics, anisotropic materials	High computational cost, especially for 3D or high-frequency simulations	Thermal, ultrasonic, mechanical simulations in CFRP and composites	Up to 95% agreement with experimental results [40,182]
Boundary Element Method (BEM)	Efficient for open-boundary electromagnetic problems	Limited to linear, simpler geometries	Eddy current testing (ECT), POD modeling	<5% impedance error compared to experiments [189]
Finite Integration Technique (FIT)	Suitable for high-frequency electromagnetic wave simulation	Limited multi-physics capabilities	Microwave and millimeter-wave NDT in CFRP	High correlation in S-parameter analysis [180]
Monte Carlo Methods	Accurate stochastic modeling for radiation transport and scattering	Computationally intensive, requires validation	Radiography testing (DRT, CRT), gamma backscatter	Improved image quality, validated by experiments [195–197]
Semi-Analytical Models	Rapid computation for specific scenarios, validation benchmarking	Limited flexibility for complex geometries	Infrared thermography, Eddy current analysis	<10% deviation from FEM/computational models [72,183]
Hybrid and Meta-Modeling Approaches	Integrates simulation, human factors, and data-driven analysis	Method-specific limitations	MAPOD, human-influenced inspection simulation	Effective simulation of human variability and POD [199,200]

4.1.4. Analytical Insights and Selection Considerations

The reviewed studies collectively demonstrate that no single modeling method is universally superior. The selection of a suitable numerical approach depends on the following:

- Type of NDT technique being modeled (ultrasonic, radiographic, electromagnetic, thermal, etc.).
- Complexity of component geometry (simple plate versus complex 3D structure).
- Nature of materials (isotropic metals vs. anisotropic composites).
- Computational resources and time constraints.

- Required output accuracy and validation requirements.
- FEM is the most versatile and widely validated method, particularly for multiphysics problems in complex composite structures.
- The BEM and semi-analytical models offer faster computations for specific electromagnetic and thermal applications, making them ideal for iterative design studies or POD evaluations.
- Monte Carlo methods are used in radiography optimization to reduce experimental exposure requirements and radiation safety risks.
- Hybrid and meta-modeling approaches provide a realistic simulation of human and environmental variability, making them valuable for risk-based decision-making frameworks, such as MAPOD.

This comparative analysis supports the strategic integration of multiple simulation methods to complement each other, thereby enhancing the reliability, efficiency, and cost-effectiveness of advanced NDT solutions for fiber-reinforced polymer materials and piping systems.

4.2. Machine Learning and Deep Learning in NDT

The rapid advancement of ML and DL has introduced transformative capabilities in NDT, particularly in automating defect detection, improving classification accuracy, and reducing operator dependence. Unlike conventional signal processing or rule-based approaches, ML and DL techniques learn from data patterns, enabling them to recognize complex defect signatures in various NDT modalities, including ultrasonic, radiographic, thermographic, and electromagnetic inspection.

4.2.1. Overview of Machine Learning Models for NDT

Recent studies have explored multiple ML algorithms, each offering unique advantages and tradeoffs. As summarized in Table 5, the commonly used models include the following:

- Support vector machines (SVM): Owing to their high classification accuracy, SVMs have been effectively applied in defect classification tasks such as identifying crack-like and pore-like defects in ultrasonic phased array images. The Poly-SVM variant demonstrated classification accuracies of up to 93%, outperforming several competing models [201–203].
- Decision trees (CART): The CART models offer high interpretability, allowing inspectors to trace the decision-making process. However, their performance may be lower than that of other models on complex datasets, owing to overfitting risks.
- K-nearest neighbors (KNN): The KNN is a simple yet powerful algorithm that classifies defects based on proximity in the feature space. Its performance depends on the choice of k and the distance metric, and it can be computationally demanding for large datasets [204,205].
- Naïve Bayes: As a probabilistic classifier, Naïve Bayes is valued for its speed and efficiency but assumes independence among features, which may not always hold in complex inspection scenarios [206,207].

Table 5. Summary of four machine learning models applied for defect classification in NDT imaging.

ML Model	Description
Support Vector Machine (SVM)	-Supervised learning algorithm for classification and regression. -Identifies the optimal hyperplane that maximizes class separation margin. -In this study, a polynomial kernel SVM (Poly-SVM) achieved the highest accuracy (93%) in classifying crack-like and pore-like defects in TFM images.
CART Decision Tree	-A tree-based supervised learning algorithm that partitions data based on feature splits. -Produces easily interpretable classification paths. -May underperform on complex datasets compared to advanced algorithms.
K-Nearest Neighbors (KNN)	-Non-parametric algorithm that classifies based on the nearest neighbors in feature space. -Highly dependent on distance metrics (e.g., Euclidean) and the choice of k-value. -Computationally intensive on large datasets.
Naive Bayes	-Probabilistic classifier based on Bayes' Theorem. -Assumes feature independence, which may not hold true in real applications. -Offers fast training but can lack accuracy on complex or correlated data.

These models have been applied in various contexts, including weld defect detection in radiographic images [208], impact damage classification in CFRP structures using thermography, and multisensor data fusion for defect characterization [209].

Successful deployment of ML models in NDT requires the availability of high-quality, accurately labeled datasets that represent a balanced distribution of defect and non-defect instances. Before model training, the collected data must undergo essential preprocessing procedures, including normalization to standardize data ranges, noise reduction to improve signal clarity, and feature extraction to convert raw sensor data into structured input suitable for ML algorithms [210]. To ensure model robustness and generalization to unseen data, the dataset should be systematically partitioned into separate training, validation, and testing sets. Finally, the trained models must be evaluated using established performance metrics such as accuracy, precision, recall, and F1-score to verify their reliability and effectiveness in practical NDT applications [209].

4.2.2. Overview of Deep Learning in NDT

DL, a subfield of ML and artificial intelligence (AI), has emerged as a transformative approach to NDT [211,212]. Unlike traditional numerical modeling or rule-based analysis, DL leverages representation learning and numerical optimization to automatically learn complex patterns from data, without requiring predefined features or handcrafted rules.

DL models, particularly deep neural networks (DNNs), consist of multiple hidden layers that hierarchically extract features from the raw data. This architecture enables them to handle high-dimensional inputs, such as images, waveforms, and sensor signals. DL methods have demonstrated remarkable performances in classification, segmentation, and regression tasks across various NDT modalities [213,214]. The common software tools and system configurations used for the DL are listed in Table 6.

Table 6. Deep learning software frameworks and hardware platforms.

Software Frameworks	Hardware Platforms
TensorFlow: An open-source machine learning library developed by Google is widely used to build and deploy deep learning models.	Graphics processing units (GPUs): Deep learning models are computationally intensive, and GPUs with parallel processing capabilities are widely used to accelerate the training and inference of deep neural networks.
PyTorch: An open-source machine-learning library developed by Facebook's AI Research Lab is known for its flexibility and ease of use.	CPU-based systems: For small-scale or less computationally demanding applications, deep learning models can also be deployed on regular CPU-based systems, especially for inference.
Keras: A high-level neural network API that runs on top of TensorFlow, providing a user-friendly interface for building deep-learning models.	Cloud-based services: Major cloud providers (e.g., AWS, Google Cloud, Microsoft Azure) offer GPU-accelerated virtual machines and managed services for training and deploying deep-learning models.
Caffe/Caffe2: Open-source deep learning frameworks often used for computer vision applications.	Edge devices: Deep learning inference can be performed on edge devices, such as embedded systems, mobile phones, and IoT devices, leveraging specialized hardware, such as tensor processing units (TPUs) or edge AI chips.
MXNet: A flexible and efficient library for deep learning that supports multiple programming languages.	

Recent studies have demonstrated the effectiveness of DL in enabling automated defect detection, segmentation, and classification using various NDT techniques. For example, Hena et al. [215] applied a U-Net segmentation model to DRT images, specifically investigating how the signal-to-noise ratio (SNR) and contrast-to-noise ratio (CNR) influence the defect recognition performance. Fotouhi et al. [216] explored autonomous damage classification in composite materials using several DL architectures, including AlexNet, ResNet-50, and custom convolutional neural networks (CNNs) [217]. Among these, AlexNet achieved the highest accuracy, ranging from 87% to 96%, in identifying damage types and severities.

Wei et al. [218] contributed by developing the PVC-Infrared dataset for pulsed thermography applications and evaluating the performance of DL-based instance segmentation models on this dataset. Their findings showed that appropriate data reduction techniques could minimize the dataset size without compromising segmentation accuracy. In the UT domain, Virkkunen et al. [219] demonstrated that incorporating data augmentation through virtual flaw generation significantly improved DL model performance, allowing it to achieve human-level accuracy in flaw detection.

Trouvé-Peloux et al. [220] applied semantic segmentation neural networks to UT C-scan data and showed that these DL methods outperformed traditional unsupervised machine learning and classical analysis techniques in accurately localizing defects in composite materials. Similarly, Yosifov et al. [221] compared traditional segmentation algorithms, such as k-means clustering, watershed, and Otsu thresholding, with DL-based models, such as U-Net and V-Net, on XCT data. Their study demonstrated that DL methods achieved superior defect detection limits and improved the POD curve estimation.

In the area of thermographic analysis, Wei et al. [222] developed DL models for detecting impact damage in curved CFRP laminates using mid-wave and long-wave infrared thermography, achieving F1-scores of 92.7% and 87.4%, respectively. Guo et al. [223] applied the InceptionTime DL architecture to AET data, achieving approximately 99% classification accuracy in identifying various damage modes, including fiber breakage, matrix cracking,

and delamination. Finally, Du et al. [224] advanced casting defect detection in X-ray images by integrating feature pyramid networks.

Effective deployment of DL models in NDT depends on the availability of large, diverse datasets that are accurately annotated to reflect various defect types and conditions. To improve model generalization and address data limitations, data augmentation techniques such as geometric transformations or noise injection are commonly applied to expand the training dataset. During the model development phase, strategies such as dropout regularization, early stopping, and cross-validation are essential to prevent overfitting and ensure the model performs reliably on unseen data [221]. Given the computational intensity of training DNNs, access to specialized hardware resources such as GPUs or cloud-based platforms is often necessary to achieve practical training times and scalable deployment in real-world inspection scenarios [225].

4.2.3. Practical Integration of ML and DL into NDT Workflows

Although these models demonstrate strong technical capabilities, their practical value is maximized when integrated into complete NDT workflows. A typical digital-physical NDT process involves the following stages.

1. Virtual inspection planning using simulation
   Numerical methods such as FEM, BEM, or FIT are used to simulate defect responses and optimize inspection parameters before physical testing.
2. Physical Data Acquisition
   Standard NDT techniques, such as PAUT, IRT, XCT, and ECT, are employed to collect raw inspection data, including ultrasonic waveforms, thermal images, and radiographic projections.
3. Data Preprocessing and Feature Extraction
   Raw signals or images are pre-processed to extract relevant features such as amplitude, frequency content, temperature gradients, or geometric descriptors.
4. Machine Learning-Based Defect Classification
   The pre-processed features are fed into ML models such as SVM, KNN, CART, or Naïve Bayes to automatically classify the type, location, and severity of detected defects. This step significantly reduces human interpretation efforts and standardizes defect assessments.
5. Model Validation and Performance Tuning
   ML models are trained and validated using historical datasets or synthetic data generated from simulations to ensure robustness and generalizability to real-world inspections.
6. Integration with digital twin and predictive maintenance platforms
   Advanced workflows may further integrate ML outputs with digital twin models or IoT sensor networks, thereby enabling real-time monitoring, predictive maintenance, and lifecycle management.

4.2.4. Deployment Considerations, Data Management, and Industrial Integration

Although ML and DL have shown promising results in controlled studies, achieving practical and scalable industrial deployment requires addressing several operational and data management challenges. Real-time processing capability is a critical requirement, particularly for applications where inspection speed and decision-making are time-sensitive. Optimizing model inference speed and computational efficiency ensures that ML and DL models can be deployed on embedded systems, edge devices, or integrated directly into NDT equipment without causing operational delays.

Seamless integration into existing inspection workflows requires compatibility with various data acquisition systems, NDT software platforms, and industrial digital twin

environments. Models must be packaged in a way that allows them to interact with live sensor data streams, enabling automated defect detection and real-time decision support. Furthermore, establishing closed-loop feedback mechanisms is essential to continuously update models with new inspection data, improving model robustness and adapting to changes in material types, defect characteristics, and operating conditions.

Data management also plays a crucial role in ensuring the reliability and sustainability of ML and DL-based NDT solutions. Organizations must implement secure and structured data storage solutions that facilitate easy retrieval and traceability. Metadata documentation, such as sensor configuration, inspection conditions, and labeling criteria should accompany datasets to ensure reproducibility and auditability. Compliance with data privacy and industry-specific regulations is also essential when handling sensitive or proprietary inspection data.

To fully leverage the potential of ML and DL in predictive maintenance and lifecycle management, these models should be integrated with broader asset management systems, including digital twins and IoT-based monitoring platforms. By doing so, organizations can transition from reactive maintenance practices to proactive and predictive strategies, reducing downtime, improving safety, and optimizing asset performance over their entire lifecycle.

4.2.5. Advantages and Challenges of ML and DL Integration in NDT

The reviewed studies collectively demonstrate that ML and DL techniques offer significant potential for transforming NDT practices across a wide range of materials, defect types, and inspection modalities. Both ML and DL contribute to automating complex data interpretation, significantly reducing inspection time and operator dependency. DL techniques, in particular, achieve high classification and segmentation accuracy, with reported performances reaching up to 99% in identifying defects, such as cracks, porosity, delamination, and impact damage.

These methods further enable the automation of feature extraction, eliminate the need for manual feature engineering, and enhance detection consistency. Their scalability across various NDT data types, including ultrasonic waveforms, radiographic images, infrared thermograms, and acoustic emission signals, makes them applicable in a wide range of industrial scenarios, including FRP pipes and composite structures.

In addition to improving defect detection performance, ML and DL models support enhanced decision-making through MAPOD studies. These frameworks integrate simulation and experimental data to provide quantitative reliability assessments, ensuring that inspection procedures meet the regulatory and safety requirements.

Moreover, the compatibility of ML and DL with Industry 4.0 frameworks positions these technologies as key enablers of real-time monitoring, predictive maintenance, and digital asset management. By integrating advanced data analytics with IoT sensor networks and digital twin platforms, organizations can shift from reactive to proactive maintenance strategies, thereby improving asset reliability and operational efficiency.

However, these benefits are challenging to achieve. The limited availability of high-quality, labeled training datasets, especially for specialized applications such as FRP pipes, remains a significant barrier to their widespread adoption. In addition, the computational demands of training deep models require access to specialized hardware or cloud-based platforms, which may not be readily available to all organizations. Overcoming these challenges will require further research, industry collaboration, and the development of application-specific datasets and validation protocols.

5. Summary and Discussion

The integration of digital technologies into NDT methods has revolutionized the detection of defects in composite materials, enabling faster and more accurate assessments. This literature review highlights significant advancements in NDT performance through the application of numerical modeling, simulation, ML, and DL.

Numerical modeling and simulation techniques, particularly FEM, have been pivotal for enhancing NDT capabilities. The FEM has been extensively employed to analyze the behavior of complex materials under various conditions. For instance, studies demonstrating the effects of thermal loads on fire-damaged reinforced concrete structures illustrate FEM's effectiveness in predicting structural failure. Similarly, FEM has been used to characterize the mechanical behavior of CFRP laminates under quasi-static tensile and fatigue loading, with findings showing good agreement between the experimental and numerical results. This alignment underscores the reliability of the method for predicting crack initiation and propagation, which is critical for assessing the integrity of composite structures.

Additionally, the use of commercial software such as COMSOL and ANSYS has facilitated advanced numerical modeling. Researchers have effectively simulated the thermal response of CFRP specimens using COMSOL, whereas others have validated comprehensive modeling approaches for additively manufactured composites, indicating the robust applicability of these tools in practical scenarios.

Moreover, the enhancement of RT through numerical modeling has streamlined the design of DRT systems, allowing for efficient system development with minimal experimental testing. The effective simulation of computed radiography techniques using the GEANT4 GATE toolkit further exemplifies how numerical modeling can optimize traditional NDT methods.

Turning to ML, both ML and DL have emerged as transformative tools in the realm of NDT. Various ML algorithms, including NN and XGB, have been successfully used to predict the mechanical properties of composite materials, showing high predictive accuracy, particularly for VIG-type composite panels. The integration of pulsed thermography with ML has further advanced the automated detection and classification of impact damage in CFRP structures, revealing that ML approaches can outperform conventional statistical analysis methods.

The application of advanced image-processing techniques combined with ML methods for weld defect detection has also shown promising results. For instance, the MSVM classifier effectively identifies and classifies a range of weld defects, underscoring the potential of ML to enhance inspection accuracy in critical applications.

DL methodologies have taken these advancements further, particularly for automated defect recognition. Research exploring the use of DL neural networks for DRT images has revealed how image quality parameters such as SNR and CNR significantly influence the performance of models such as U-Net. Additionally, DL approaches have demonstrated high accuracy in classifying the types and severities of composite damage, making them valuable for real-time inspection applications.

5.1. Comparative Performance Analysis

To evaluate the effectiveness of the various digital approaches reviewed, Table 7 presents a comparative summary of reported performance outcomes. These include quantitative metrics such as accuracy, POD, F1-scores, and improvement percentages for both modeling- and AI-based techniques.

Table 7. Summary of reported accuracy and performance improvements in advanced NDT techniques.

NDT Technique	Digital Enhancement Method	Reported Performance Metric	Reference
Phased Array Ultrasonic Testing (PAUT)	FEM-based simulation and MAPOD	90% probability of detecting defects ≥1 mm at 95% confidence	[200]
Microwave NDT (MWNDT)	FIT and FEM simulation	Accurate S-parameter variation correlated with damage states in CFRP	[180]
Infrared Thermography (IRT)	FEM and GRU Deep Learning	>90% defect depth quantification accuracy	[40]
Eddy Current Testing (ECT)	BEM with Gaussian modeling	Impedance prediction with <5% error	[189]
Radiography Testing (DRT/CRT)	Monte Carlo simulation (GATE Toolkit)	Improved image quality and 30% reduction in exposure time	[195,196]
Ultrasonic TFM Imaging	Poly-SVM ML classification	93% accuracy in classifying crack-like and pore-like defects	[226]
Thermographic Damage Detection	Cube SVM ML classification	78.7–93.5% accuracy in CFRP damage detection	[210]
Radiographic Weld Inspection	MSVM ML classification	High precision in multi-class weld defect detection	[208]
Composite Damage Detection	CNN (AlexNet) DL classification	87–96% accuracy in damage type and severity classification	[216]
Pulsed Thermography	DL instance segmentation	Data reduction with maintained segmentation performance	[218]
Ultrasonic Flaw Detection	DL with virtual flaw data augmentation	Human-level performance in flaw detection	[219]
UT C-scan Defect Localization	Semantic segmentation DL models	Superior defect localization compared to traditional ML	[220]
XCT Image Analysis	U-Net and V-Net DL segmentation	Enhanced POD curve estimation and defect detection limits	[221]
Impact Damage in CFRP	DL models on midwave and longwave IRT data	F1-scores of 92.7% (midwave) and 87.4% (longwave)	[222]
Acoustic Emission Analysis	InceptionTime DL classification	~99% accuracy in fiber breakage, matrix cracking, and delamination detection	[223]
Casting Defect Detection	FPN and RoIAlign DL models	23.6% improvement over Faster R-CNN in small defect localization	[224]

5.2. Key Observations and Industrial Implications

Several key trends emerge from the performance analysis in Table 7.

- Simulation-based techniques (e.g., FEM, BEM, and Monte Carlo) offer reliable pre-inspection planning tools, enabling the optimization of sensor configuration, parameter tuning, and MAPOD evaluation.
- ML methods provide effective solutions for feature-based defect classification, particularly when well-labeled data are available.
- DL approaches are effective in handling large and complex datasets, achieving state-of-the-art performance in classification and segmentation, particularly in imaging-based NDT (e.g., radiography, infrared, and ultrasonic C-scan).

- The combination of simulation and AI methods allows for synergistic workflows such as training ML models on synthetic defect data generated from simulations.
- These approaches are increasingly compatible with Industry 4.0, offering opportunities for real-time monitoring, predictive maintenance, and digital twin integration.

These capabilities are particularly important in FRP pipe systems. Given the anisotropy, multi-layered construction, and curvature of FRP components, traditional NDT methods often struggle with sensitivity and consistency. Advanced digital tools provide the flexibility and accuracy required for early defect detection, automated interpretation, and lifecycle reliability assessment.

Despite these benefits, several challenges remain. These include application-specific datasets, model interpretability, computational resource requirements, and industrial-scale validation. Future work should focus on bridging these gaps by developing open-access defect libraries, refining hybrid simulation-AI frameworks, and deploying field-ready NDT solutions tailored to FRP pipe applications.

6. Conclusions

This comprehensive review has critically examined the state-of-the-art advancements in digital technologies for NDT of FRP pipes, with a particular focus on the roles of numerical simulation, ML, and DL in enhancing defect detection, classification, and system reliability. Sections 4 and 5 demonstrate that while conventional NDT methods provide foundational capabilities, they fall short when confronted with the inherent complexity, anisotropy, and multiscale defect mechanism characteristics of FRP pipe systems.

The integration of FEM, BEM, and probabilistic modeling has emerged as a paradigm shift, enabling predictive defect behavior analysis, optimization of inspection strategies, and MAPOD assessments with minimized experimental dependency. The application of ML and DL algorithms, ranging from SVM and CNN architectures to advanced semantic segmentation models, has demonstrated remarkable performance in automating defect characterization, reducing human bias, and accelerating data-driven decision-making processes.

However, despite these technological breakthroughs, the review underscores a critical research gap: the limited translation of these digital NDT advancements into field-deployable solutions specifically optimized for FRP piping infrastructure. The unique challenges posed by the layered, anisotropic, and often large-scale nature of FRP pipelines necessitate tailored NDT methodologies that extend beyond generic composite material applications. Furthermore, the scarcity of high-fidelity, domain-specific datasets coupled with the lack of standardized validation frameworks for FRP pipe inspection hinders the widespread adoption of these advanced methods in real-world industrial environments.

To bridge this gap, future research must prioritize the development of integrated digital twin frameworks that combine real-time sensor data, high-resolution simulation models, and AI-driven analytics for the continuous structural health monitoring of FRP pipelines. Collaborative efforts between academia, industry, and standardization bodies are essential for establishing benchmark datasets, validation protocols, and best practices tailored to FRP piping systems. Moreover, advancing explainable AI techniques will be pivotal to ensuring transparency, interpretability, and regulatory acceptance of ML- and DL-based NDT systems.

In summary, although digital and AI-enhanced NDT techniques have demonstrated exceptional potential, their full realization in the context of FRP pipes requires a concerted shift toward application-specific research, validated deployment strategies, and cross-disciplinary collaboration. Such advancements will not only elevate the integrity management of FRP piping assets, but also contribute to the broader digital transformation of the composite materials industry.

Author Contributions: Conceptualization, J.L.T., M.T.H.S. and A.Ł.; methodology, J.L.T., F.S.S., J.J. and Z.O.; software, J.L.T.; validation, M.T.H.S., A.Ł., J.J., Z.O. and F.S.S.; formal analysis, J.L.T., M.T.H.S., J.J. and A.Ł.; investigation, J.L.T. and F.S.S.; resources, J.L.T.; data curation, J.L.T.; writing—original draft preparation, J.L.T.; writing—review and editing, M.T.H.S., A.Ł., J.J., Z.O. and F.S.S.; visualization, J.L.T.; supervision, M.T.H.S., A.Ł., J.J., Z.O. and F.S.S.; project administration, F.S.S.; funding acquisition, M.T.H.S., J.J., A.Ł. and Z.O. All authors have read and agreed to the published version of the manuscript.

Funding: The authors are grateful for the financial support given by The Ministry of Higher Education Malaysia (MOHE) under the Higher Institution Centre of Excellence (HICOE2.0/5210004) at the Institute of Tropical Forestry and Forest Products. The paper is co-financed from the funds of the state budget under the program of the Minister of Science under the name Polish Metrology II Programme, project number No. PM-II/SP/0040/2024/02 entitled "Multisensor system for measuring thermo-mechanical interactions together with a comprehensive analysis of the state", amount of funding PLN 968,000.00, total project value PLN 968,000.00, Poland. The paper is co-financed from the funds of the state budget under the program of the Minister of Science under the name Polish Metrology II Programme, project no. PM-II/SP/0093/2024/02 entitled "Building the algorithms of blind signal processing based on geometrical structure of information". Founding amount: PLN 966,800.00. The total value of the project is PLN 966,800.00, Poland. This research was partially financed by the Ministry of Science and Higher Education of Poland with allocation to the Faculty of Mechanical Engineering, Bialystok University of Technology, for the WZ/WM-IIM/5/2023 and WZ/WM-IIB/4/2023 academic projects in the mechanical engineering and biomedical engineering disciplines.

Data Availability Statement: No new data were created in this study.

Acknowledgments: The authors would also like to express their gratitude to the Department of Aerospace Engineering, Faculty of Engineering, Universiti Putra Malaysia, and the Laboratory of Biocomposite Technology, Institute of Tropical Forestry and Forest Product (INTROP), Universiti Putra Malaysia (HICOE) for their close collaboration in this study.

Conflicts of Interest: The authors declare no conflicts of interest.

References

1. Tai, J.L.; Sultan, M.T.H.; Shahar, F.S. Experimental Study on the Efficacy of Ultrasound in In-Situ Detection of Corrosion in Palm Oil Refining Equipment. *J. Teknol.* **2024**, *86*, 151–159. [CrossRef]
2. Vanaei, H.R.; Eslami, A.; Egbewande, A. A Review on Pipeline Corrosion, in-Line Inspection (ILI), and Corrosion Growth Rate Models. *Int. J. Press. Vessel. Pip.* **2017**, *149*, 43–54. [CrossRef]
3. Amoah, P.; Owusu-Poku, S.; Ajubala, G.A. Investigation of Wall Thickness, Corrosion, and Deposits in Industrial Pipelines Using Radiographic Technique. *Int. J. Corros.* **2023**, *2023*, 4924399. [CrossRef]
4. Mu, W.; Gao, Y.; Wang, Y.; Liu, G.; Hu, H. Modeling and Analysis of Acoustic Emission Generated by Fatigue Cracking. *Sensors* **2022**, *22*, 1208. [CrossRef]
5. Tanvir, F.; Sattar, T.; Mba, D.; Edwards, G. Identification of Fatigue Damage Evaluation Using Entropy of Acoustic Emission Waveform. *SN Appl. Sci.* **2020**, *2*, 138. [CrossRef]
6. Guan, R.; Lu, Y.; Wang, K.; Su, Z. Quantitative Fatigue Crack Evaluation in Pipeline Structures Using Nonlinear Cylindrical Waves. *Smart Mater. Struct.* **2019**, *28*, 025015. [CrossRef]
7. Tai, J.L.; Sultan, M.T.H.; Shahar, F.S. Processing Plants Damage Mechanisms and On-Stream Inspection Using Phased Array Corrosion Mapping—A Systematic Review. *Pertanika J. Sci. Technol.* **2024**, *32*, 1665–1685. [CrossRef]
8. Przemysław Sobkiewicz; Bienkowski, P.; Błazejewski, W. Microwave Non-Destructive Testing for Delamination Detection in Layered Composite Pipelines. *Sensors* **2021**, *21*, 4168. [CrossRef]
9. Li, X.K.; Liu, P.F. Delamination Analysis of Carbon Fiber Composites Under Dynamic Loads Using Acoustic Emission. *J. Fail. Anal. Prev.* **2016**, *16*, 142–153. [CrossRef]
10. Lecheb, S.; Daoui, A.; Brihmat, C.; Mechakra, H.; Chellil, A.; Safi, B.; Kebir, H. Study of Composite Pipelines Damaged by Corrosion: Control by Non-Destructive Testing. *Hung. J. Ind. Chem.* **2023**, *51*, 1–6. [CrossRef]
11. Xin, M.L.; Chen, Y.; Li, M.D.; Wang, Z.G.; Gu, G.H. The Research of Penetration Testing in the FRP Pipe Applications. *IOP Conf. Ser. Mater. Sci. Eng.* **2018**, *292*, 012080. [CrossRef]

12. Matsukawa, S.; Yoshida, K.; Okuda, T.; Hazama, M.; Kurokawa, S.; Murata, H. Non-Destructive Inspection Method for FRPM Pipelines Utilising Time-Domain Responses of Microwave Guided-Modes. *Electron. Lett.* **2020**, *56*, 982–985. [CrossRef]
13. Malla, P.; Khedmatgozar Dolati, S.S.; Ortiz, J.D.; Mehrabi, A.B.; Nanni, A.; Dinh, K. Feasibility of Conventional Non-Destructive Testing Methods in Detecting Embedded FRP Reinforcements. *Appl. Sci.* **2023**, *13*, 4399. [CrossRef]
14. Zhang, T.; Mahdi, M.; Issa, M.; Xu, C.; Ozevin, D. Experimental Study on Monitoring Damage Progression of Basalt-FRP Reinforced Concrete Slabs Using Acoustic Emission and Machine Learning. *Sensors* **2023**, *23*, 8356. [CrossRef]
15. Brizuela, J.; Camacho, J.; Cosarinsky, G.; Iriarte, J.M.; Cruza, J.F. Improving Elevation Resolution in Phased-Array Inspections for NDT. *NDT E Int.* **2019**, *101*, 1–16. [CrossRef]
16. Martín-Díaz, C.; Rubio-Cintas, M.D.; Benaissa, K. Ndt Techniques Applied for the Inspection of Flare Stacks. *Int. J. Ind. Eng. Res. Dev.* **2018**, *9*, 1–12. [CrossRef]
17. Montinaro, N.; Cerniglia, D.; Pitarresi, G. Evaluation of Interlaminar Delaminations in Titanium-Graphite Fibre Metal Laminates by Infrared NDT Techniques. *NDT E Int.* **2018**, *98*, 134–146. [CrossRef]
18. Matalgah, K.; Ravindranath, P.K.; Pulipati, D.; Fleck, T.J. Automated Quantification of Interlaminar Delaminations in Carbon-Fiber-Reinforced Polymers via High-Resolution Ultrasonic Testing. *Polymers* **2023**, *15*, 4691. [CrossRef]
19. Jasiūnienė, E.; Mažeika, L.; Samaitis, V.; Cicėnas, V.; Mattsson, D. Ultrasonic Non-Destructive Testing of Complex Titanium/Carbon Fibre Composite Joints. *Ultrasonics* **2019**, *95*, 13–21. [CrossRef]
20. Ibrahim, M.E. Ultrasonic Inspection of Hybrid Polymer Matrix Composites. *Compos. Sci. Technol.* **2021**, *208*, 5–13. [CrossRef]
21. Rizwan, M.K.; Laureti, S.; Mooshofer, H.; Goldammer, M.; Ricci, M. Ultrasonic Imaging of Thick Carbon Fiber Reinforced Polymers through Pulse-Compression-Based Phased Array. *Appl. Sci.* **2021**, *11*, 1508. [CrossRef]
22. Tai, J.L.; Sultan, M.T.H.; Shahar, F.S. Comparative Analysis of Ultrasonic Inspection Techniques for Corrosion Monitoring in Petrochemical Plants Using Analytic Hierarchy Process (AHP). *Pertanika J. Sci. Technol.* **2025**, *33*, 1439–1457. [CrossRef]
23. Anoshkin, A.N.; Osokin, V.M.; Tretyakov, A.A.; Potrakhov, N.N.; Bessonov, V.B. Application of Operational Radiographic Inspection Method for Flaw Detection of Blade Straightener from Polymeric Composite Materials. *J. Phys. Conf. Ser.* **2017**, *808*, 012003. [CrossRef]
24. Kusk, M.W.; Jensen, J.M.; Gram, E.H.; Nielsen, J.; Precht, H. Anode Heel Effect: Does It Impact Image Quality in Digital Radiography? A Systematic Literature Review. *Radiography* **2021**, *27*, 976–981. [CrossRef]
25. Xu Feng, L.; Jie, S.; Lu, S.; Wang, L. Application of On-Line Digital Radiographic Inspection for Pipeline with Insulation. *J. Phys. Conf. Ser.* **2022**, *2366*, 012006. [CrossRef]
26. Gholizadeh, S. A Review of Non-Destructive Testing Methods of Composite Materials. *Procedia Struct. Integr.* **2016**, *1*, 50–57. [CrossRef]
27. Pacana, A.; Siwiec, D.; Bednárová, L. Method of Choice: A Fluorescent Penetrant Taking into Account Sustainability Criteria. *Sustainability* **2020**, *12*, 5854. [CrossRef]
28. Endramawan, T.; Sifa, A. Non Destructive Test Dye Penetrant and Ultrasonic on Welding SMAW Butt Joint with Acceptance Criteria ASME Standard. *IOP Conf. Ser. Mater. Sci. Eng.* **2018**, *306*, 012122. [CrossRef]
29. Vera, J.; Caballero, L.; Taboada, M. Reliability of Dye Penetrant Inspection Method to Detect Weld Discontinuities. *Russ. J. Nondestruct. Test.* **2024**, *60*, 85–95. [CrossRef]
30. Šofer, M.; Cienciala, J.; Fusek, M.; Pavlicek, P.; Moravec, R. Damage Analysis of Composite CFRP Tubes Using Acoustic Emission Monitoring. *Materials* **2021**, *14*, 786. [CrossRef]
31. Oliveira, T.L.L.; Bortoluzzi, D.B.; Barbosa, L.C.M.; Ancelotti, A.C. Acoustic Emission Analysis of Mode II Interlaminar Fracture Toughness of 3D Reinforced CFRP. *NDT* **2024**, *2*, 32–52. [CrossRef]
32. Samborski, S.; Korzec, I. Application of the Acoustic Emission Technique for Damage Identification in the Fiber Reinforced Polymer Composites. *Adv. Sci. Technol. Res. J.* **2023**, *17*, 210–221. [CrossRef]
33. Ghadarah, N.; Ayre, D. A Review on Acoustic Emission Testing for Structural Health Monitoring of Polymer-Based Composites. *Sensors* **2023**, *23*, 6945. [CrossRef]
34. Barile, C.; Casavola, C.; Pappalettera, G.; Kannan, V.P. Application of Different Acoustic Emission Descriptors in Damage Assessment of Fiber Reinforced Plastics: A Comprehensive Review. *Eng. Fract. Mech.* **2020**, *235*, 107083. [CrossRef]
35. Hamam, Z.; Godin, N.; Fusco, C.; Doitrand, A.; Monnier, T. Acoustic Emission Signal Due to Fiber Break and Fiber Matrix Debonding in Model Composite: A Computational Study. *Appl. Sci.* **2021**, *11*, 8406. [CrossRef]
36. Bashkov, O.V.; Romashko, R.V.; Zaikov, V.I.; Panin, S.V.; Bezruk, M.N.; Khun, K.; Bashkov, I.O. Detecting Acoustic-Emission Signals with Fiber-Optic Interference Transducers. *Russ. J. Nondestruct. Test.* **2017**, *53*, 415–421. [CrossRef]
37. Ghahremani, P.; Najafabadi, M.A.; Alimirzaei, S.; Fotouhi, M. Acoustic Emission-Based Analysis of Damage Mechanisms in Filament Wound Fiber Reinforced Composite Tubes. *Sensors* **2023**, *23*, 6994. [CrossRef]
38. Saeedifar, M.; Zarouchas, D. Damage Characterization of Laminated Composites Using Acoustic Emission: A Review. *Compos. B Eng.* **2020**, *195*, 108039. [CrossRef]

39. Tai, J.L.; Sultan, M.T.H.; Łukaszewicz, A.; Siemiątkowski, Z.; Skorulski, G.; Shahar, F.S. Preventing Catastrophic Failures: A Review of Applying Acoustic Emission Testing in Multi-Bolted Flanges. *Metals* **2025**, *15*, 438. [CrossRef]
40. Fang, Q.; Maldague, X. A Method of Defect Depth Estimation for Simulated Infrared Thermography Data with Deep Learning. *Appl. Sci.* **2020**, *10*, 6819. [CrossRef]
41. Qu, Z.; Jiang, P.; Zhang, W. Development and Application of Infrared Thermography Non-Destructive Testing Techniques. *Sensors* **2020**, *20*, 3851. [CrossRef]
42. Liu, K.; Ma, Z.; Liu, Y.; Yang, J.; Yao, Y. Enhanced Defect Detection in Carbon Fiber Reinforced Polymer Composites via Generative Kernel Principal Component Thermography. *Polymers* **2021**, *13*, 825. [CrossRef]
43. Pitarresi, G.; Scalici, T.; Catalanotti, G. Infrared Thermography Assisted Evaluation of Static and Fatigue Mode II Fracture Toughness in FRP Composites. *Compos. Struct.* **2019**, *226*, 111220. [CrossRef]
44. Tai, J.L.; Sultan, M.T.H.; Shahar, F.S.; Łukaszewicz, A.; Oksiuta, Z.; Grzejda, R. Ultrasound Corrosion Mapping on Hot Stainless Steel Surfaces. *Metals* **2024**, *14*, 1425. [CrossRef]
45. Yosifov, M.; Reiter, M.; Heupl, S.; Gusenbauer, C.; Fröhler, B.; Fernández- Gutiérrez, R.; De Beenhouwer, J.; Sijbers, J.; Kastner, J.; Heinzl, C. Probability of Detection Applied to X-Ray Inspection Using Numerical Simulations. *Nondestruct. Test. Eval.* **2022**, *37*, 536–551. [CrossRef]
46. Chen, H.X.; Fan, D.L.; Fang, L.; Zhang, G.Y.; Cao, C.H.; Huang, W.J.; Huang, J.M.; Yang, L. Finite Element Numerical Simulation Analysis Based on Ultrasonic Phased Array. *IOP Conf. Ser. Mater. Sci. Eng.* **2019**, *657*, 012011. [CrossRef]
47. Le Noir de Carlan, M.; Jason, L.; Davenne, L. Numerical Simulation of Anchor Pullout and Shear Tests Using a Regularized Damage Model. *Appl. Sci.* **2024**, *14*, 11262. [CrossRef]
48. Efimov, A.G.; Kanter, B.M.; Kuzelev, N.R.; Martyanov, E.V.; Shubochkin, A.E. Numerical Simulation of Non-Destructive Remote Field Eddy Current Testing of Rolled Metal Tubes. *J. Phys. Conf. Ser.* **2019**, *1327*, 012012. [CrossRef]
49. Ciaburro, G.; Iannace, G. Machine-Learning-Based Methods for Acoustic Emission Testing: A Review. *Appl. Sci.* **2022**, *12*, 10476. [CrossRef]
50. Yang, Q.; Liu, Y.; Chen, T.; Tong, Y. Federated Machine Learning: Concept and Applications. *ACM Trans. Intell. Syst. Technol.* **2019**, *10*, 12. [CrossRef]
51. Lei, Y.; Yang, B.; Jiang, X.; Jia, F.; Li, N.; Nandi, A.K. Applications of Machine Learning to Machine Fault Diagnosis: A Review and Roadmap. *Mech. Syst. Signal Process* **2020**, *138*, 106587. [CrossRef]
52. Zhang, Z.; Tang, F.; Cao, Q.; Pan, H.; Wang, X.; Lin, Z. Deep Learning-Enriched Stress Level Identification of Pretensioned Rods via Guided Wave Approaches. *Buildings* **2022**, *12*, 1772. [CrossRef]
53. Inderyas, O.; Alver, N.; Tayfur, S.; Shimamoto, Y.; Suzuki, T. Deep Learning-Based Acoustic Emission Signal Filtration Model in Reinforced Concrete. *Arab. J. Sci. Eng.* **2024**, *50*, 1885–1903. [CrossRef]
54. Fu, Y.; Zhu, G.; Zhu, M.; Xuan, F. Digital Twin for Integration of Design-Manufacturing-Maintenance: An Overview. *Chin. J. Mech. Eng. (Engl. Ed.)* **2022**, *35*, 80. [CrossRef]
55. Attaran, M.; Celik, B.G. Digital Twin: Benefits, Use Cases, Challenges, and Opportunities. *Decis. Anal. J.* **2023**, *6*, 100165. [CrossRef]
56. Tao, F.; Zhang, H.; Liu, A.; Nee, A.Y.C. Digital Twin in Industry: State-of-the-Art. *IEEE Trans. Ind. Inform.* **2019**, *15*, 2405–2415. [CrossRef]
57. Sharma, A.; Kosasih, E.; Zhang, J.; Brintrup, A.; Calinescu, A. Digital Twins: State of the Art Theory and Practice, Challenges, and Open Research Questions. *J. Ind. Inf. Integr.* **2022**, *30*, 100383. [CrossRef]
58. Kim, F.H.; Pintar, A.; Obaton, A.F.; Fox, J.; Tarr, J.; Donmez, A. Merging Experiments and Computer Simulations in X-Ray Computed Tomography Probability of Detection Analysis of Additive Manufacturing Flaws. *NDT E Int.* **2021**, *119*, 102416. [CrossRef]
59. Falcetelli, F.; Yue, N.; Rossi, L.; Bolognini, G.; Bastianini, F.; Zarouchas, D.; Di Sante, R. A Model-Assisted Probability of Detection Framework for Optical Fiber Sensors. *Sensors* **2023**, *23*, 4813. [CrossRef]
60. Lee, D.; Yoon, S.; Park, J.; Eum, S.; Cho, H. Demonstration of Model-Assisted Probability of Detection Framework for Ultrasonic Inspection of Cracks in Compressor Blades. *NDT E Int.* **2022**, *128*, 102618. [CrossRef]
61. Chipanga, T.; Nemraoui, O.; Ismail, F. Damage Assessment of Low-Velocity Impacted Sandwich Composite Structures Using X-Ray Micro-Computed Tomography. *J. Eng.* **2024**, *2024*, 6147948. [CrossRef]
62. Zhao, X.; Li, J.; Su, S.; Jiang, N. Prediction Models of Mechanical Properties of Jute/PLA Composite Based on X-Ray Computed Tomography. *Polymers* **2024**, *16*, 160. [CrossRef]
63. Tsamos, A.; Evsevleev, S.; Fioresi, R.; Faglioni, F.; Bruno, G. Synthetic Data Generation for Automatic Segmentation of X-Ray Computed Tomography Reconstructions of Complex Microstructures. *J. Imaging* **2023**, *9*, 22. [CrossRef]
64. Ziółkowski, G.; Pach, J.; Pyka, D.; Kurzynowski, T.; Jamroziak, K. X-Ray Computed Tomography for the Development of Ballistic Composite. *Materials* **2020**, *13*, 5566. [CrossRef] [PubMed]

65. Antin, K.N.; Machado, M.A.; Santos, T.G.; Vilaça, P. Evaluation of Different Non-Destructive Testing Methods to Detect Imperfections in Unidirectional Carbon Fiber Composite Ropes. *J. Nondestruct. Eval.* **2019**, *38*, 23. [CrossRef]
66. Taheri, H.; Hassen, A.A. Nondestructive Ultrasonic Inspection of Composite Materials: A Comparative Advantage of Phased Array Ultrasonic. *Appl. Sci.* **2019**, *9*, 1628. [CrossRef]
67. Mohd Tahir, M.F.; Echtermeyer, A.T. Phased Array Ultrasonic Testing on Thick Glass Fiber Reinforced Thermoplastic Composite Pipe Implementing the Classical Time-Corrected Gain Method. *J. Nondestruct. Eval.* **2024**, *43*, 74. [CrossRef]
68. Camineroa, M.A.; García-Morenoa, I.; Rodrígueza, G.P.; Chacónb, J.M. Internal Damage Evaluation of Composite Structures Using Phased Array Ultrasonic Technique: Impact Damage Assessment in CFRP and 3D Printed Reinforced Composites. *Compos. B Eng.* **2018**, *165*, 131–142. [CrossRef]
69. Tai, J.L.; Grzejda, R.; Sultan, M.T.H.; Łukaszewicz, A.; Shahar, F.S.; Tarasiuk, W.; Rychlik, A. Experimental Investigation on the Corrosion Detectability of A36 Low Carbon Steel by the Method of Phased Array Corrosion Mapping. *Materials* **2023**, *16*, 5297. [CrossRef]
70. Pelkner, M.; Casperson, R.; Pohl, R.; Munzke, D.; Becker, B. Eddy Current Testing of Composite Pressure Vessels. *Int. J. Appl. Electromagn. Mech.* **2019**, *59*, 1221–1226. [CrossRef]
71. Abdelli, D.E.; Nguyen, T.T.; Clenet, S.; Cheriet, A. Stochastic Metamodel for Probability of Detection Estimation of Eddy-Current Testing Problem in Random Geometric. *IEEE Trans. Magn.* **2019**, *55*, 6200604. [CrossRef]
72. Apostol, E.S.; Nedelcu, A.; Daniel, D.V.; Chiriţă, I.; Tănase, N. Mathematical Modeling of Eddy Current Non-Destructive Testing. In Proceedings of the 2017 10th International Symposium on Advanced Topics in Electrical Engineering (ATEE 2017), Bucharest, Romania, 23–25 March 2017; pp. 469–474. [CrossRef]
73. To, A.; Li, Z.; Dixon, S. Improved Detection of Surface Defects at Sample Edges Using High-Frequency Eddy Current Amplitude and Phase Measurements. *Nondestruct. Test. Eval.* **2022**, *37*, 795–819. [CrossRef]
74. Cao, B.; Li, X.; Wang, M.; Fan, M. Analytical Modelling and Simulations for High-Frequency Eddy Current Testing with Planar Spiral Coils. *Nondestruct. Test. Eval.* **2021**, *36*, 195–208. [CrossRef]
75. Tytko, G.; Adamczyk-Habrajska, M.; Li, Y.; Liu, Z.; Kopec, M. High Frequency Eddy Current Method in Inspection of Aluminide Coatings Integrity after Simulating Service Loads. *Measurement* **2025**, *252*, 117356. [CrossRef]
76. Švantner, M.; Muzika, L.; Moskovchenko, A.; Pereira, C.M.C.; Das, S. Repeatability Study of Flash-Pulse Thermographic Inspection of CFRP Samples. *Eng. Proc.* **2021**, *8*, 1. [CrossRef]
77. Pirinu, A.; Saponaro, A.; Nobile, R.; Panella, F.W. Low-Velocity Impact Damage Quantification on Sandwich Panels by Thermographic and Ultrasonic Procedures. *Exp. Tech.* **2024**, *48*, 299–322. [CrossRef]
78. Peeters, J.; Ibarra-Castanedo, C.; Khodayar, F.; Mokhtari, Y.; Sfarra, S.; Zhang, H.; Maldague, X.; Dirckx, J.J.J.; Steenackers, G. Optimised Dynamic Line Scan Thermographic Detection of CFRP Inserts Using FE Updating and POD Analysis. *NDT E Int.* **2018**, *93*, 141–149. [CrossRef]
79. Tai, J.L.; Sultan, M.T.H.; Łukaszewicz, A.; Shahar, F.S.; Oksiuta, Z.; Krishnamoorthy, R.R. Enhancing Turnaround Maintenance in Process Plants through On-Stream Phased Array Corrosion Mapping: A Review. *Appl. Sci.* **2024**, *14*, 6707. [CrossRef]
80. De Almeida, P.D.; Pereira, G.R. Phased Array Inspection of Glass Fiber Reinforced Polymers Pipeline Joints. *J. Mater. Res. Technol.* **2019**, *8*, 4736–4740. [CrossRef]
81. Hao, Z.; Liu, H.; Yan, N.; Wang, Z.; Bai, X.; Han, J.; Mi, C.; Jia, S.; Sun, G.; Zhu, L.; et al. In-Situ Test and Numerical Simulation of Anchoring Performance of Embedded Rock GFRP Anchor. *Buildings* **2023**, *13*, 2799. [CrossRef]
82. Shu, W.; Liao, L.; Zhou, P.; Huang, B.; Chen, W. Three-Point Bending Damage Detection of GFRP Composites Doped with Graphene Oxide by Acoustic Emission Technology. *iScience* **2023**, *26*, 108511. [CrossRef] [PubMed]
83. Nair, A.; Cai, C.S.; Kong, X. Using Acoustic Emission to Monitor Failure Modes in CFRP-Strengthened Concrete Structures. *J. Aerosp. Eng.* **2020**, *33*, 04019110. [CrossRef]
84. Mills-Dadson, B.; Tran, D.; Asamene, K.; Whitlow, T.; Sundaresan, M. Acoustic Emission Monitoring of Unstable Damage Growth in CFRP Composites under Tension. *AIP Conf. Proc.* **2017**, *1806*, 070009.
85. Luo, Z.; Li, F.; Su, H.; Cao, H.; Lin, L. Surface Adaptive Ultrasonic Testing on Defects in CFRP Radii. *Jixie Gongcheng Xuebao/J. Mech. Eng.* **2022**, *58*, 312–318. [CrossRef]
86. Xiao, H.; Sultan, M.T.H.; Shahar, F.S.; Gaff, M.; Hui, D. Recent Developments in the Mechanical Properties of Hybrid Fiber Metal Laminates in the Automotive Industry: A Review. *Rev. Adv. Mater. Sci.* **2023**, *62*, 20220328. [CrossRef]
87. Liu, Y.; Natsuki, T.; Suzuki, D.; Huang, C.; Cui, L.; Ni, Q.Q. Low-Velocity Impact-Resistance of Aramid Fiber Three-Dimensional Woven Textile-Reinforced Thermoplastic-Epoxy Composites. *J. Thermoplast. Compos. Mater.* **2023**, *37*, 2827–2857. [CrossRef]
88. Zhang, B.; Jia, L.; Tian, M.; Ning, N.; Zhang, L.; Wang, W. Surface and Interface Modification of Aramid Fiber and Its Reinforcement for Polymer Composites: A Review. *Eur. Polym. J.* **2021**, *147*, 110352. [CrossRef]
89. Liu, H.; Yu, Y.; Liu, Y.; Zhang, M.; Li, L.; Ma, L.; Sun, Y.; Wang, W. A Review on Basalt Fiber Composites and Their Applications in Clean Energy Sector and Power Grids. *Polymers* **2022**, *14*, 2376. [CrossRef]

90. Selcuk, S.; Ahmetoglu, U.; Gokce, E.C. Basalt Fiber Reinforced Polymer Composites (BFRP) Other than Rebars: A Review. *Mater. Today Commun.* **2023**, *37*, 107359. [CrossRef]
91. Song, K.; Yu, Y.; Liu, Y.; Zhao, J. Flexural Performance Study of Basalt-Fiber-Reinforced Polymer Bar Basalt-Fiber-Reinforced Concrete Beams. *Buildings* **2023**, *13*, 2583. [CrossRef]
92. Vinay, S.S.; Sanjay, M.R.; Siengchin, S.; Venkatesh, C.V. Basalt Fiber Reinforced Polymer Composites Filled with Nano Fillers: A Short Review. *Mater. Today Proc.* **2022**, *52*, 2460–2466. [CrossRef]
93. Loganathan, T.M.; Sultan, M.T.H.; Muhammad Amir, S.M.; Jamil, J.; Yusof, M.R.; Md Shah, A.U. Infrared Thermographic and Ultrasonic Inspection of Randomly-Oriented Short-Natural Fiber-Reinforced Polymeric Composites. *Front. Mater.* **2021**, *7*, 604459. [CrossRef]
94. Zhang, H.; Sfarra, S.; Sarasini, F.; Santulli, C.; Fernandes, H.; Avdelidis, N.P.; Ibarra-Castanedo, C.; Maldague, X.P.V. Thermographic Non-Destructive Evaluation for Natural Fiber-Reinforced Composite Laminates. *Appl. Sci.* **2018**, *8*, 240. [CrossRef]
95. Wang, Z.; Chegdani, F.; Yalamarti, N.; Takabi, B.; Tai, B.; El Mansori, M.; Bukkapatnam, S. Acoustic Emission Characterization of Natural Fiber Reinforced Plastic Composite Machining Using a Random Forest Machine Learning Model. *J. Manuf. Sci. Eng. Trans. ASME* **2020**, *142*, 031003. [CrossRef]
96. Chen, J.; Yu, Z.; Jin, H. Nondestructive Testing and Evaluation Techniques of Defects in Fiber-Reinforced Polymer Composites: A Review. *Front. Mater.* **2022**, *9*, 986645. [CrossRef]
97. Joseph, L.; Madhavan, M.K.; Jayanarayanan, K.; Pegoretti, A. Evaluation of Hybrid Fiber Multiscale Polymer Composites for Structural Confinement under Cyclic Axial Compressive Loading. *J. Compos. Sci.* **2023**, *7*, 152. [CrossRef]
98. Singh, P.; Singari, R.M.; Mishra, R.S.; Bajwa, G.S. A Review on Recent Development on Polymeric Hybrid Composite and Analysis of Their Enhanced Mechanical Performance. *Mater. Today Proc.* **2022**, *56*, 3692–3701. [CrossRef]
99. Bafakeeh, O.T.; Shewakh, W.M.; Abu-Oqail, A.; Abd-Elaziem, W.; Abdel Ghafaar, M.; Abu-Okail, M. Synthesis and Characterization of Hybrid Fiber-Reinforced Polymer by Adding Ceramic Nanoparticles for Aeronautical Structural Applications. *Polymers* **2021**, *13*, 4116. [CrossRef]
100. Bruno, M.; Esposito, L.; Papa, I.; Viscusi, A. Design, Manufacturing, and Numerical Characterization of Hybrid Fiber Reinforced Polymer under Dynamic Loads. *J. Mater. Eng. Perform.* **2023**, *32*, 3905–3913. [CrossRef]
101. Bhaskar, R.; Reddivari, S.; Vadapalli, B.; Sanduru, T.; Buddi, K.; Maksudovna, V.; Joshi, A.; Reddy Reddivari, B.; Vadapalli, S.; Sanduru, B.; et al. Fabrication and Mechanical Properties of Hybrid Fibre-Reinforced Polymer Hybrid Composite with Graphene Nanoplatelets and Multiwalled Carbon Nanotubes. *Cogent Eng.* **2024**, *11*, 2343586. [CrossRef]
102. Islam, T.; Chaion, M.H.; Jalil, M.A.; Rafi, A.S.; Mushtari, F.; Dhar, A.K.; Hossain, S. Advancements and Challenges in Natural Fiber-Reinforced Hybrid Composites: A Comprehensive Review. *SPE Polym.* **2024**, *5*, 481–506. [CrossRef]
103. Mohanraj, C.M.; Rameshkumar, R.; Mariappan, M.; Mohankumar, A.; Rajendran, B.; Senthamaraikannan, P.; Suyambulingam, I.; Kumar, R. Recent Progress in Fiber Reinforced Polymer Hybrid Composites and Its Challenges—A Comprehensive Review. *J. Nat. Fibers* **2025**, *22*, 2495911. [CrossRef]
104. Bannister, A.; Nemcova, A.; Johnson, D.; Blackburn, M. Selection and Deployment of Non-Destructive Testing for through-Life Integrity Assurance of Composite-Repaired Pipes. *Inst. Chem. Eng. Symp. Ser.* **2020**, *2020*, 1–14.
105. Mousa, S.; Alomari, A.S.; Vantadori, S.; Alhazmi, W.H.; Abd-Elhady, A.A.; Sallam, H.E.D.M. Mechanical Behavior of Epoxy Reinforced by Hybrid Short Palm/Glass Fibers. *Sustainability* **2022**, *14*, 9425. [CrossRef]
106. Pranathi, K.; Md, S.; Ayub, A.; Paul, C.H.; Singh, S.; Hanumantharaju, H.G.; Ravi, S.; Yadla, T.; Nagaraj Goud, B.; Vyshnavi, V.; et al. An Experimental Study on E-Glass Fiber Reinforced Epoxy with Nano-Silica for an Aircraft Structural Applications. *J. Phys. Conf. Ser.* **2024**, *2837*, 012004. [CrossRef]
107. Bhanuprakash, L.; Varghese, S.; Singh, S.K. Glass Fibre Reinforced Epoxy Composites Modified with Graphene Nanofillers: Electrical Characterization. *J. Nanomater.* **2022**, *2022*, 4611251. [CrossRef]
108. Subbarayalu, V.; Chinnaraman, S.; Ayyanar, A.; Chinnapalanisamy, J.; Subbarayalu, V.; Chinnaraman, S.; Ayyanar, A.; Chinnapalanisamy, J. Mechanical Properties of Vinyl Ester Hybrid Composite Laminates Reinforced with Screw Pine and Glass Fiber. *AIMS Mater. Sci.* **2024**, *11*, 114–128. [CrossRef]
109. Thomason, J.; Xypolias, G. A Study of the Moisture Absorption Characteristics of Vinyl Ester Polymer and Unidirectional Glass Fibre Vinyl Ester Laminates. *J. Compos. Sci.* **2024**, *8*, 214. [CrossRef]
110. Gupta, B.N.V.S.K.G.; Yadav, A.; Hiremath, M.M.; Prusty, R.K.; Ray, B.C. Enhancement of Mechanical Properties of Glass Fiber Reinforced Vinyl Ester Composites by Embedding Multi-Walled Carbon Nanotubes through Solution Processing Technique. *Mater. Today Proc.* **2020**, *27*, 1045–1050. [CrossRef]
111. Thomason, J.; Xypolias, G. Hydrothermal Ageing of Glass Fibre Reinforced Vinyl Ester Composites: A Review. *Polymers* **2023**, *15*, 835. [CrossRef]
112. Nazaruddin, N.; Akram, A.; Hasanuddin, I.; Iqbal, M.; Kurniawan, R.; Putra, R. Mechanical Properties of Glass Fiber Reinforced Polyester Resin for Use as the Wall of the Acehnese Boat 'Thep-Thep'. *IOP Conf. Ser. Mater. Sci. Eng.* **2019**, *523*, 012080. [CrossRef]

113. Singh, M.M.; Kumar, H.; Kumar, G.H.; Sivaiah, P.; Nagesha, K.V.; Ajay, K.M.; Vijaya, G. Determination of Strength Parameters of Glass Fibers Reinforced Composites for Engineering Applications. *Silicon* **2020**, *12*, 1–11. [CrossRef]
114. Abbood, I.S.; Odaa, S.A.; Hasan, K.F.; Jasim, M.A. Properties Evaluation of Fiber Reinforced Polymers and Their Constituent Materials Used in Structures—A Review. *Mater. Today Proc.* **2021**, *43*, 1003–1008. [CrossRef]
115. Setyanto, D.; Jayatun, Y.A.; Basoeki, P.D.; De Fretes, A. Physical Properties of Glass-Fibre-Reinforced Polymer Filled with Alumina Trihydrate and Calcium Carbonate. *Polymers* **2022**, *14*, 2464. [CrossRef]
116. Hu, B.; Shen, S.; Zhai, M.; Zhao, N.; Huang, H.; Duan, Y.; Ma, J.; Wan, T.; Shao, W.; Zhang, Q. Development of Thermoplastic Epoxy Resin-Based Multifunctional Flexible Composite Film and Its Shape Memory Performance Research. *Mater. Today Commun.* **2024**, *40*, 109842. [CrossRef]
117. Wu, J.; Li, C.; Hailatihan, B.; Mi, L.; Baheti, Y.; Yan, Y. Effect of the Addition of Thermoplastic Resin and Composite on Mechanical and Thermal Properties of Epoxy Resin. *Polymers* **2022**, *14*, 1087. [CrossRef]
118. Miranda, R.; Luciano, M.; Fiore, V.; Valenza, A. Development of Bio-Based and Recyclable Epoxy Adhesives by Modification with Thermoplastic Polymers. *Polymers* **2025**, *17*, 131. [CrossRef]
119. Bhagwat, Y.; Nayak, G.; Pandit, P.; Lakshmi, A. Effect of Polypropylene Fibres on Strength and Durability Performance of M-Sand Self Compacting Concrete. *Cogent Eng.* **2023**, *10*, 2233783. [CrossRef]
120. Wu, J.; Hu, L.; Hu, C.; Wang, Y.; Zhou, J.; Li, X. Impact of Polypropylene Fiber on the Mechanical and Physical Properties of Pervious Concrete: An Experimental Investigation. *Buildings* **2023**, *13*, 1966. [CrossRef]
121. Hedjazi, S.; Castillo, D. Utilizing Polypropylene Fiber in Sustainable Structural Concrete Mixtures. *CivilEng* **2022**, *3*, 562–572. [CrossRef]
122. Saberian, M.; Tajaddini, A.; Li, J.; Zhang, G.; Wang, L.; Sun, D.; Maqsood, T.; Roychand, R. Mechanical Properties of Polypropylene Fibre Reinforced Recycled Concrete Aggregate for Sustainable Road Base and Subbase Applications. *Constr. Build. Mater.* **2023**, *405*, 133352. [CrossRef]
123. Yao, X.; Han, Y.; Shen, L.; Zhu, D. Experimental Study on the Effect of Polypropylene Fiber on Compressive Strength and Fracture Properties of High-Strength Concrete after Elevated Temperatures. *J. Build. Eng.* **2024**, *86*, 108860. [CrossRef]
124. Suraweera, S.M.D.V.; De Silva, S. Effect of Recycled Polyethylene Terephthalate (PET) Fibres on Fresh and Hardened Properties of Concrete: A Review. *Int. J. Sustain. Eng.* **2023**, *16*, 269–284. [CrossRef]
125. Özaşik, N.; Eren, Ö. Influence of Recycled Polyethylene Terephthalate Fibres on Plastic Shrinkage and Mechanical Properties of Concrete. *Front. Struct. Civ. Eng.* **2022**, *16*, 792–802. [CrossRef]
126. Ma, J.; Hesp, S.A.M. Effect of Recycled Polyethylene Terephthalate (PET) Fiber on the Fracture Resistance of Asphalt Mixtures. *Constr. Build. Mater.* **2022**, *342*, 127944. [CrossRef]
127. Gnoffo, C.; Arrigo, R.; Frache, A. An Upcycling Strategy for Polyethylene Terephthalate Fibers: All-Polymer Composites with Enhanced Mechanical Properties. *J. Compos. Sci.* **2024**, *8*, 527. [CrossRef]
128. Zhou, Z.; Li, S.; Hu, G.; Wu, J.; Yao, C.; Niu, F. On the Use of Recycled Polyethylene Terephthalate Fiber in One-Part Geopolymer Stabilized Soft Soil: Tensile Performance and Sustainability Analysis. *Dev. Built Environ.* **2025**, *21*, 100641. [CrossRef]
129. Molinar-Díaz, J.; Parsons, A.J.; Ahmed, I.; Warrior, N.A.; Harper, L.T. Poly-Ether-Ether-Ketone (PEEK) Biomaterials and Composites: Challenges, Progress, and Opportunities. *Polym. Rev.* **2024**, *65*, 527–565. [CrossRef]
130. Lee, S.; Jeon, I.S.; Jho, J.Y. Mechanical Properties of Polyetheretherketone Composites with Surface-Modified Hydroxyapatite Nanofibers and Carbon Fibers. *Macromol. Res.* **2022**, *30*, 261–270. [CrossRef]
131. Lu, S.; Zhang, B.; Niu, J.; Yang, C.; Sun, C.; Wang, L.; Li, D. High-Strength Carbon Fiber-Reinforced Polyether-Ether-Ketone Composites with Longer Fiber Retention Length Manufactured via Screw Extrusion-Based 3D Printing. *Addit. Manuf.* **2024**, *86*, 104200. [CrossRef]
132. Dai, J.N.; Kou, S.Q.; Yang, H.Y.; Xu, Z.B.; Shu, S.L.; Qiu, F.; Jiang, Q.C.; Zhang, L.C. High-Content Continuous Carbon Fibers Reinforced PEEK Matrix Composite with Ultra-High Mechanical and Wear Performance at Elevated Temperature. *Compos. Struct.* **2022**, *295*, 115837. [CrossRef]
133. Eun, J.H.; Choi, B.K.; Sung, S.M.; Kim, M.S.; Lee, J.S. Effect of Toughened Polyamide-Coated Carbon Fiber Fabric on the Mechanical Performance and Fracture Toughness of CFRP. *J. Compos. Mater.* **2021**, *55*, 2721–2738. [CrossRef]
134. Kohutiar, M.; Kakošová, L.; Krbata, M.; Janík, R.; Fekiač, J.J.; Breznická, A.; Eckert, M.; Mikuš, P.; Timárová, Ľ. Comprehensive Review: Technological Approaches, Properties, and Applications of Pure and Reinforced Polyamide 6 (PA6) and Polyamide 12 (PA12) Composite Materials. *Polymers* **2025**, *17*, 442. [CrossRef]
135. Jafari, M.M.; Jahandari, S.; Ozbakkaloglu, T.; Rasekh, H.; Jahed Armaghani, D.; Rahmani, A. Mechanical Properties of Polyamide Fiber-Reinforced Lime–Cement Concrete. *Sustainability* **2023**, *15*, 11484. [CrossRef]
136. Ai, L.; Flowers, S.; Mesaric, T.; Henderson, B.; Houck, S.; Ziehl, P. Acoustic Emission-Based Detection of Impacts on Thermoplastic Aircraft Control Surfaces: A Preliminary Study. *Appl. Sci.* **2023**, *13*, 6573. [CrossRef]

137. Balakrishnan, T.S.; Sultan, M.T.H.; Naveen, J.; Shahar, F.S.; Najeeb, M.I.; Shah, A.U.M.; Khan, T.; Sebaey, T.A. Selection of Natural Fibre for Pultruded Hybrid Synthetic/Natural Fibre Reinforced Polymer Composites Using Analytical Hierarchy Process for Structural Applications. *Polymers* **2022**, *14*, 3178. [CrossRef] [PubMed]
138. Saghir, F.; Gohari, S.; Mozafari, F.; Moslemi, N.; Burvill, C.; Smith, A.; Lucas, S. Mechanical Characterization of Particulated FRP Composite Pipes: A Comprehensive Experimental Study. *Polym. Test.* **2021**, *93*, 107001. [CrossRef]
139. Ashrith, H.S.; Jeevan, T.P.; Xu, J. A Review on the Fabrication and Mechanical Characterization of Fibrous Composites for Engineering Applications. *J. Compos. Sci.* **2023**, *7*, 252. [CrossRef]
140. Rajak, D.K.; Wagh, P.H.; Linul, E. Manufacturing Technologies of Carbon/Glass Fiber-Reinforced Polymer Composites and Their Properties: A Review. *Polymers* **2021**, *13*, 3721. [CrossRef]
141. Agwa, M.A.; Youssef, S.M.; Ali-Eldin, S.S.; Megahed, M. Integrated Vacuum Assisted Resin Infusion and Resin Transfer Molding Technique for Manufacturing of Nano-Filled Glass Fiber Reinforced Epoxy Composite. *J. Ind. Text.* **2022**, *51*, 5113S–5144S. [CrossRef]
142. Shen, R.; Liu, T.; Liu, H.; Zou, X.; Gong, Y.; Guo, H. An Enhanced Vacuum-Assisted Resin Transfer Molding Process and Its Pressure Effect on Resin Infusion Behavior and Composite Material Performance. *Polymers* **2024**, *16*, 1386. [CrossRef]
143. Wang, T.; Huang, K.; Guo, L.; Zheng, T.; Zeng, F. An Automated Vacuum Infusion Process for Manufacturing High-Quality Fiber-Reinforced Composites. *Compos. Struct.* **2023**, *309*, 116717. [CrossRef]
144. Shah, M.; Chaudhary, V. Flow Modeling and Simulation Study of Vacuum Assisted Resin Transfer Molding (VARTM) Process: A Review. *IOP Conf. Ser. Mater. Sci. Eng.* **2020**, *872*, 012087. [CrossRef]
145. Liu, Y.N.; Yuan, C.; Liu, C.; Pan, J.; Dong, Q. Study on the Resin Infusion Process Based on Automated Fiber Placement Fabricated Dry Fiber Preform. *Sci. Rep.* **2019**, *9*, 7440. [CrossRef] [PubMed]
146. Phyo Maung, P.; Lin Htet, T.; Malysheva, G.V. Simulation and Optimization of Vacuum Assisted Resin Infusion Process for Large-Sized Structures Made of Carbon Fiber-Reinforced Plastics. *IOP Conf. Ser. Mater. Sci. Eng.* **2020**, *709*, 022041. [CrossRef]
147. Shi, J.; Zhang, W.; Zhang, J.; Yuan, S.; Chen, H. Mechanical, Thermal Properties and Void Characteristics of Bamboo Fiber-Reinforced Epoxy Resin Composites Prepared by Vacuum-Assisted Resin Transfer Molding Process. *J. Nat. Fibers* **2023**, *20*, 2187919. [CrossRef]
148. Lionetto, F.; Moscatello, A.; Totaro, G.; Raffone, M.; Maffezzoli, A. Experimental and Numerical Study of Vacuum Resin Infusion of Stiffened Carbon Fiber Reinforced Panels. *Materials* **2020**, *13*, 4800. [CrossRef] [PubMed]
149. Aryaswara, L.G.; Santos, G.N.C.; Muflikhun, M.A. Defect Characteristics of Unidirectional Glass Fiber Reinforced Epoxy Manufactured via Vacuum Assisted Resin Infusion. *Mater. Today Proc.* **2022**, *66*, 2796–2800. [CrossRef]
150. Silva, D.; Rocha, R.; Ribeiro, F.; Monteiro, H. Environmental Impact of an Innovative Aeronautic Carbon Composite Manufactured via Heated Vacuum-Assisted Resin Transfer Molding. *Sustainability* **2024**, *16*, 3253. [CrossRef]
151. Kim, J.I.; Hwang, Y.T.; Choi, K.H.; Kim, H.J.; Kim, H.S. Prediction of the Vacuum Assisted Resin Transfer Molding (VARTM) Process Considering the Directional Permeability of Sheared Woven Fabric. *Compos. Struct.* **2019**, *211*, 236–243. [CrossRef]
152. Liu, X.; Cao, Y.; Zhang, C.; Zhou, L.; Gao, Y.; Wang, W.; Guan, H.; Mu, S.; Zhang, J. Study on Mechanical Properties of Vacuum-Infused Glass Fiber Reinforced Thermoplastic Methacrylic Resin Composites. *Polym. Compos.* **2024**, *45*, 7024–7038. [CrossRef]
153. Bobba, S.; Leman, Z.; Zainuddin, E.S.; Sapuan, S.M. Failures Analysis of E-Glass Fibre Reinforced Pipes in Oil and Gas Industry: A Review. *IOP Conf. Ser. Mater. Sci. Eng.* **2017**, *217*, 012004. [CrossRef]
154. Kong, L.; Shi, Q.; Zhang, B. Experimental Analysis of a Novel GFRP Stiffened Pipe. *Appl. Sci.* **2022**, *12*, 10306. [CrossRef]
155. Diniță, A.; Ripeanu, R.G.; Ilincă, C.N.; Cursaru, D.; Matei, D.; Naim, R.I.; Tănase, M.; Portoacă, A.I. Advancements in Fiber-Reinforced Polymer Composites: A Comprehensive Analysis. *Polymers* **2024**, *16*, 2. [CrossRef]
156. Kennedy, S.M.; Jeen Robert, R.B.; Malkiya Rasalin Prince, R.; Hikku, G.S.; Kaliraj, M. A Comprehensive Overview of the Fabrication and Testing Methods of FRP Composite Pipes. *MethodsX* **2024**, *13*, 102990. [CrossRef]
157. Alabtah, F.G.; Mahdi, E.; Eliyan, F.F. The Use of Fiber Reinforced Polymeric Composites in Pipelines: A Review. *Compos. Struct.* **2021**, *276*, 114595. [CrossRef]
158. Wang, B.; Zhong, S.; Lee, T.L.; Fancey, K.S.; Mi, J. Non-Destructive Testing and Evaluation of Composite Materials/Structures: A State-of-the-Art Review. *Adv. Mech. Eng.* **2020**, *12*, 1–28. [CrossRef]
159. Lewis, C.; Yavuz, B.O.; Longana, M.L.; Belnoue, J.P.H.; Ramakrishnan, K.R.; Ward, C.; Hamerton, I. A Review on the Modelling of Aligned Discontinuous Fibre Composites. *J. Compos. Sci.* **2024**, *8*, 318. [CrossRef]
160. Mehdikhani, M.; Gorbatikh, L.; Verpoest, I.; Lomov, S.V. Voids in Fiber-Reinforced Polymer Composites: A Review on Their Formation, Characteristics, and Effects on Mechanical Performance. *J. Compos. Mater.* **2019**, *53*, 1579–1669. [CrossRef]
161. Ma, M.; Cao, H.; Jiang, M.; Sun, L.; Zhang, L.; Zhang, F.; Sui, Q.; Tian, A.; Liang, J.; Jia, L. High Precision Detection Method for Delamination Defects in Carbon Fiber Composite Laminates Based on Ultrasonic Technique and Signal Correlation Algorithm. *Materials* **2020**, *13*, 3840. [CrossRef]

162. Ellison, A.; Kim, H. Shadowed Delamination Area Estimation in Ultrasonic C-Scans of Impacted Composites Validated by X-Ray CT. *J. Compos. Mater.* **2020**, *54*, 549–561. [CrossRef]
163. Yi, Q.; Tian, G.Y.; Malekmohammadi, H.; Zhu, J.; Laureti, S.; Ricci, M. New Features for Delamination Depth Evaluation in Carbon Fiber Reinforced Plastic Materials Using Eddy Current Pulse-Compression Thermography. *NDT E Int.* **2019**, *102*, 264–273. [CrossRef]
164. Laureti, S.; Khalid Rizwan, M.; Malekmohammadi, H.; Burrascano, P.; Natali, M.; Torre, L.; Rallini, M.; Puri, I.; Hutchins, D.; Ricci, M. Delamination Detection in Polymeric Ablative Materials Using Pulse-Compression Thermography and Air-Coupled Ultrasound. *Sensors* **2019**, *19*, 2198. [CrossRef]
165. Drummer, J.; Tafesh, F.; Fiedler, B. Effect of Fiber Misalignment and Environmental Temperature on the Compressive Behavior of Fiber Composites. *Polymers* **2023**, *15*, 2833. [CrossRef] [PubMed]
166. Jafarypouria, M.; Lomov, S.V.; Mahato, B.; Abaimov, S.G. The Effect of Fibre Misalignment in an Impregnated Fibre Bundle on Stress Concentrations. *Compos. Part. A Appl. Sci. Manuf.* **2024**, *178*, 108001. [CrossRef]
167. Aggarwal, S.; Kumar, K.; Aggarwal, M.L. Analysis of Glass Fiber-Reinforced Composite Leaf Springs in a Light Commercial Vehicle. *Sci. Rep.* **2024**, *14*, 20126. [CrossRef] [PubMed]
168. Coca-Gonzalez, M.; Jimenez-Martinez, M. Warpage: Causes, Manufacturing Processes and Future Challenges: A Review. *Proc. Inst. Mech. Eng. Part L J. Mater. Des. Appl.* **2024**, 1–17. [CrossRef]
169. Collins, C.; Batista, N.L.; Hubert, P. Warpage Investigation of Carbon/PEEK Discontinuous Long Fibre Thin Panels. *J. Compos. Mater.* **2021**, *55*, 3529–3537. [CrossRef]
170. Diaz, M.; Baur, J.W. Warpage of Thin Additively Manufactured Continuous Fiber Thermoset Composites. *Addit. Manuf.* **2025**, *102*, 104749. [CrossRef]
171. Amaguaña, M.; Guamán, L.; Gómez, N.B.Y.; Khorami, M.; Calvo, M.; Albuja-Sánchez, J. Test Method for Studying the Shrinkage Effect under Controlled Environmental Conditions for Concrete Reinforced with Coconut Fibres. *Materials* **2023**, *16*, 3247. [CrossRef]
172. Aghaee, K.; Khayat, K.H. Effect of Shrinkage-Mitigating Materials on Performance of Fiber-Reinforced Concrete—An Overview. *Constr. Build. Mater.* **2021**, *305*, 124586. [CrossRef]
173. Aghaee, K.; Khayat, K.H. Design and Performance of Fiber-Reinforced Shrinkage Compensating Eco-Friendly Concrete. *Constr. Build. Mater.* **2023**, *408*, 133803. [CrossRef]
174. Saradar, A.; Tahmouresi, B.; Mohseni, E.; Shadmani, A. Restrained Shrinkage Cracking of Fiber-Reinforced High-Strength Concrete. *Fibers* **2018**, *6*, 12. [CrossRef]
175. Sui, J.; Li, X.; Zhang, H.; Xu, F.; Deng, J.; Hu, R.; Chen, M. Effect of Different Fibers on Shrinkage Properties and Bonding Properties of Geopolymer Mortar Repair Materials and Analysis of the Mechanism. *Coatings* **2023**, *13*, 1542. [CrossRef]
176. Łukaszewicz, A. Nonlinear Numerical Model of Friction Heating during Rotary Friction Welding. *J. Frict. Wear* **2018**, *39*, 476–482. [CrossRef]
177. Sidun, P.; Łukaszewicz, A. Verification of Ram-Press Pipe Bending Process Using Elasto-Plastic FEM Model. *Acta Mech. Autom.* **2017**, *11*, 47–52. [CrossRef]
178. Łukaszewicz, A. Temperature Field in the Contact Zone in the Course of Rotary Friction Welding of Metals. *Mater. Sci.* **2019**, *55*, 39–45. [CrossRef]
179. Acharjee, D.; Bandyopadhyay, D. A Numerical Study on the Fire Induced Collapse of a Real Life Warehouse Structure Based on Post-Fire NDT Results. *J. Mines Met. Fuels* **2023**, *71*, 1235–1249. [CrossRef]
180. Munalli, D.; Dimitrakis, G.; Chronopoulos, D.; Greedy, S.; Long, A. The Use of Free-Space Microwave Non-Destructive Techniques_ Simulation of Damage Detection in Carbon Fibre Reinforced Composites. In Proceedings of the 11th Symposium on NDT in Aerospace, Paris, France, 13–15 November 2019; pp. 1–10.
181. Evans, E.E.; Brooks, R.A.; Liu, J.; Hall, Z.E.C.; Liu, H.; Lowe, T.J.E.; Withers, P.J.; Kinloch, A.J.; Dear, J.P. Comparison of X-Ray Computed Tomography and Ultrasonic C-Scan Techniques and Numerical Modelling of Impact Damage in a CFRP Composite Laminate. *Appl. Compos. Mater.* **2024**, *31*, 249–264. [CrossRef]
182. Feito, N.; Calvo, J.V.; Belda, R.; Giner, E. An Experimental and Numerical Investigation to Characterize an Aerospace Composite Material with Open-Hole Using Non-Destructive Techniques. *Sensors* **2020**, *20*, 4148. [CrossRef]
183. Ratsakou, A.; Reboud, C.; Skarlatos, A.; Lesselier, D. Fast Simulation Approach Dedicated to Infrared Thermographic Inspection of Delaminated Planar Pieces. *AIP Conf. Proc.* **2019**, *2102*, 120004. [CrossRef]
184. Notebaert, A.; Quinten, J.; Moonens, M.; Olmez, V.; Barros, C.; Cunha, S.S.; Demarbaix, A. Numerical Modelling of the Heat Source and the Thermal Response of an Additively Manufactured Composite during an Active Thermographic Inspection. *Materials* **2024**, *17*, 13. [CrossRef]
185. Kim, H.J.; Shrestha, R.; Pradhan, S.S.; Gurung, P.; Bhattarai, P.; Lamichhane, N.; Kim, C.S.; Shrestha, R. Modelling and Simulation for Defect Detection in Hydroelectric Penstock Using Infrared Thermography. *Therm. Sci. Eng.* **2023**, *6*, 2494. [CrossRef]

186. Marrazzo, M.; Sharif Khodaei, Z.; Aliabadi, M.H.F. Laplace Domain Boundary Element Method for Structural Health Monitoring of Poly-Crystalline Materials at Micro-Scale. *Appl. Sci.* **2023**, *13*, 13138. [CrossRef]
187. Bao, Y.; Liu, Z.; Bowler, J.R.; Song, J. Nested Kernel Degeneration-Based Boundary Element Method Solver for Rapid Computation of Eddy Current Signals. *NDT E Int.* **2022**, *128*, 102633. [CrossRef]
188. Tai, J.L.; Sultan, M.T.H.; Shahar, F.S.; Yidris, N.; Basri, A.A.; Md Shah, A.U. Exploring Probability of Detection (POD) Analysis in Nondestructive Testing: A Comprehensive Review and Potential Applications in Phased Array Ultrasonic Corrosion Mapping. *Pertanika J. Sci. Technol.* **2024**, *32*, 2165–2191. [CrossRef]
189. Baskaran, P.; Pasadas, D.J.; Ramos, H.G.; Ribeiro, A.L. Integration of Multiple Response Signals into the Probability of Detection Modelling in Eddy Current NDE of Flaws. *NDT E Int.* **2021**, *118*, 102401. [CrossRef]
190. Hachi, D.; Benhadda, N.; Helifa, B.; Lefkaier, I.K.; Abdelhadi, B. Composite Material Characterization Using Eddy Current by 3D FEM Associated with Iterative Technique. *Adv. Electromagn.* **2019**, *8*, 8–15. [CrossRef]
191. Xi, Z.; Li, S.; Feng, C.; Wang, X.; Luo, X. Analytical Modeling and Non-Dimensionalization Study for Endoscopic Ultrasound Acoustic Field in Tubular Structure. *NDT E Int.* **2025**, *150*, 103275. [CrossRef]
192. Cheikh, K.; Boudi, E.L.M.; Rabi, R.; Mokhliss, H. Balancing the Maintenance Strategies to Making Decisions Using Monte Carlo Method. *MethodsX* **2024**, *13*, 102819. [CrossRef]
193. Wicaksono, F.D.; Arshad, Y.B.; Sihombing, H. Norm-Dist Monte-Carlo Integrative Method for the Improvement of Fuzzy Analytic Hierarchy Process. *Heliyon* **2020**, *6*, e03607. [CrossRef] [PubMed]
194. Yao, M.; Kaftandjian, V.; Peterzol-Parmentier, A.; Schumm, A.; Duvauchelle, P. Hybrid Monte Carlo and Deterministic Simulation Approach for Modeling a Computed Radiography Imaging Chain from X-Ray Exposure to Optical Readout. *Nucl. Instrum. Methods Phys. Res. A* **2019**, *941*, 162328. [CrossRef]
195. Mousa, T.; Taha, E.; Alnadwi, F.; Siddig, M.; Banoqitah, E. Simulation Study on X-Ray Radiographic Testing of Welds. In *Challenges and Recent Advancements in Nuclear Energy Systems—Proceedings of Saudi International Conference on Nuclear Power Engineering SCOPE*; Springer: Cham, Switzerland, 2024.
196. Sari, M.B.; Wirawan, R.; Waris, A.; Kim, H.J.; Djamal, M. Simulation of Void Detection System Using Gamma-Ray Compton Scattering Technique. *J. Eng. Technol. Sci.* **2019**, *51*, 369–379. [CrossRef]
197. Kumar, S.; Menaka, M.; Venkatraman, B. Radiographic Simulation and Validation Studies on Weld Joints of Annular Tanks and Cylindrical Tanks. *IOP Conf. Ser. Mater. Sci. Eng.* **2019**, *554*, 012008. [CrossRef]
198. Osipov, S.P.; Chakhlov, S.V.; Kairalapov, D.U.; Sirot'yan, E.V. Numerical Modeling of Radiographic Images as the Basis for Correctly Designing Digital Radiography Systems of Large-Sized Objects. *Russ. J. Nondestruct. Test.* **2019**, *55*, 136–149. [CrossRef]
199. Rodat, D.; Guibert, F.; Dominguez, N.; Calmon, P. Operational NDT Simulator, towards Human Factors Integration in Simulated Probability of Detection. *AIP Conf. Proc.* **2017**, *1806*, 140004. [CrossRef]
200. Lei, X.; Wirdelius, H.; Rosell, A. Simulation-Based Investigation of a Probability of Detection (POD) Model Using Phased Array Ultrasonic Testing (PAUT) Technique. *J. Nondestruct. Eval.* **2022**, *41*, 40. [CrossRef]
201. Vives, J.; Palací, J.; Heart, J.; Vives, J.; Palací, J.; Heart, J. SVM-Algorithm for Supervision, Monitoring and Detection Vibration in Wind Turbines. *J. Comput. Commun.* **2022**, *10*, 44–55. [CrossRef]
202. Da Silva Souza, J.; Luz Dos Santos, M.V.; Suzuki Bayma, R.; Amarante Mesquita, A.L. Analysis of Window Size and Statistical Features for SVM-Based Fault Diagnosis in Bearings. *IEEE Lat. Am. Trans.* **2021**, *19*, 243–249. [CrossRef]
203. Dobrzycki, A.; Mikulski, S.; Opydo, W. Using ANN and SVM for the Detection of Acoustic Emission Signals Accompanying Epoxy Resin Electrical Treeing. *Appl. Sci.* **2019**, *9*, 1523. [CrossRef]
204. Kiyak, E.O.; Ghasemkhani, B. High-Level K-Nearest Neighbors (HLKNN): A Supervised Machine Learning Model for Classification Analysis. *Electronics* **2023**, *12*, 3828. [CrossRef]
205. Grochowalski, J.M.; Chady, T. Rapid Identification of Material Defects Based on Pulsed Multifrequency Eddy Current Testing and the K-Nearest Neighbor Method. *Materials* **2023**, *16*, 6650. [CrossRef] [PubMed]
206. Shu, L.; Zhang, H.; You, Y.; Cui, Y.; Chen, W. Towards Fire Prediction Accuracy Enhancements by Leveraging an Improved Naïve Bayes Algorithm. *Symmetry* **2021**, *13*, 530. [CrossRef]
207. Kaushik, K.; Bhardwaj, A.; Dahiya, S.; Maashi, M.S.; Al Moteri, M.; Aljebreen, M.; Bharany, S. Multinomial Naive Bayesian Classifier Framework for Systematic Analysis of Smart IoT Devices. *Sensors* **2022**, *22*, 7318. [CrossRef]
208. Malarvel, M.; Singh, H. An Autonomous Technique for Weld Defects Detection and Classification Using Multi-Class Support Vector Machine in X-Radiography Image. *Optik* **2021**, *231*, 166342. [CrossRef]
209. Cormerais, R.; Duclos, A.; Wasselynck, G.; Berthiau, G.; Longo, R. A Data Fusion Method for Non-Destructive Testing by Means of Artificial Neural Networks. *Sensors* **2021**, *21*, 2598. [CrossRef]
210. Alhammad, M.; Avdelidis, N.P.; Ibarra-Castanedo, C.; Torbali, M.E.; Genest, M.; Zhang, H.; Zolotas, A.; Maldgue, X.P.V. Automated Impact Damage Detection Technique for Composites Based on Thermographic Image Processing and Machine Learning Classification. *Sensors* **2022**, *22*, 9031. [CrossRef]

211. Palma-Ramírez, D.; Ross-Veitía, B.D.; Font-Ariosa, P.; Espinel-Hernández, A.; Sanchez-Roca, A.; Carvajal-Fals, H.; Nuñez-Alvarez, J.R.; Hernández-Herrera, H. Deep Convolutional Neural Network for Weld Defect Classification in Radiographic Images. *Heliyon* **2024**, *10*, e30590. [CrossRef]
212. Posilović, L.; Medak, D.; Milković, F.; Subašić, M.; Budimir, M.; Lončarić, S. Deep Learning-Based Anomaly Detection from Ultrasonic Images. *Ultrasonics* **2022**, *124*, 106737. [CrossRef]
213. Park, S.K.; Kim, J.; Park, D.G.; Jo, M.; Lee, J.; Lee, J. Experimental Investigation to Improve Inspection Accuracy of Magnetic Field Imaging-Based NDT Using Deep Neural Network. *Russ. J. Nondestruct. Test.* **2022**, *58*, 732–744. [CrossRef]
214. Nele, L.; Mattera, G.; Vozza, M. Deep Neural Networks for Defects Detection in Gas Metal Arc Welding. *Appl. Sci.* **2022**, *12*, 3615. [CrossRef]
215. Hena, B.; Wei, Z.; Castanedo, C.I.; Maldague, X. Deep Learning Neural Network Performance on NDT Digital X-Ray Radiography Images: Analyzing the Impact of Image Quality Parameters—An Experimental Study. *Sensors* **2023**, *23*, 4324. [CrossRef]
216. Fotouhi, S.; Pashmforoush, F.; Bodaghi, M.; Fotouhi, M. Autonomous Damage Recognition in Visual Inspection of Laminated Composite Structures Using Deep Learning. *Compos. Struct.* **2021**, *268*, 113960. [CrossRef]
217. Cha, Y.J.; Choi, W.; Büyüköztürk, O. Deep Learning-Based Crack Damage Detection Using Convolutional Neural Networks. *Comput.-Aided Civ. Infrastruct. Eng.* **2017**, *32*, 361–378. [CrossRef]
218. Wei, Z.; Osman, A.; Valeske, B.; Maldague, X. Pulsed Thermography Dataset for Training Deep Learning Models. *Appl. Sci.* **2023**, *13*, 2901. [CrossRef]
219. Virkkunen, I.; Koskinen, T.; Jessen-Juhler, O.; Rinta-aho, J. Augmented Ultrasonic Data for Machine Learning. *J. Nondestruct. Eval.* **2021**, *40*, 4. [CrossRef]
220. Trouvé-Peloux, P.; Abeloos, B.; Ben Fekih, A.; Trottier, C.; Roche, J.M. Benefit of Neural Network for the Optimization of Defect Detection on Composite Material Using Ultrasonic Non Destructive Testing. In Proceedings of the 48th Annual Review of Progress in Quantitative Nondestructive Evaluation (QNDE 2021), Virtual, 28–30 July 2021. [CrossRef]
221. Yosifov, M.; Weinberger, P.; Reiter, M.; Fröhler, B.; De Beenhouwer, J.; Sijbers, J.; Kastner, J.; Heinzl, C. Defect Detectability Analysis via Probability of Defect Detection between Traditional and Deep Learning Methods in Numerical Simulations. *e-J. Nondestruct. Test.* **2023**, *28*, 2–11. [CrossRef] [PubMed]
222. Wei, Z.; Fernandes, H.; Herrmann, H.G.; Tarpani, J.R.; Osman, A. A Deep Learning Method for the Impact Damage Segmentation of Curve-Shaped Cfrp Specimens Inspected by Infrared Thermography. *Sensors* **2021**, *21*, 395. [CrossRef]
223. Guo, F.; Li, W.; Jiang, P.; Chen, F.; Yang, C. Deep Learning Approach for Damage Classification Based on Acoustic Emission Data in Composite Materials. *Materials* **2022**, *15*, 4270. [CrossRef]
224. Du, W.; Shen, H.; Fu, J.; Zhang, G.; He, Q. Approaches for Improvement of the X-Ray Image Defect Detection of Automobile Casting Aluminum Parts Based on Deep Learning. *NDT E Int.* **2019**, *107*, 102144. [CrossRef]
225. Pointon, J.L.; Wen, T.; Tugwell-Allsup, J.; Sújar, A.; Létang, J.M.; Vidal, F.P. Simulation of X-Ray Projections on GPU: Benchmarking GVirtualXray with Clinically Realistic Phantoms. *Comput. Methods Programs Biomed.* **2023**, *234*, 107500. [CrossRef] [PubMed]
226. Wang, H.; Fan, Z.; Chen, X.; Cheng, J.; Chen, W.; Wang, Z.; Bu, Y. Automated Classification of Pipeline Defects from Ultrasonic Phased Array Total Focusing Method Imaging. *Energies* **2022**, *15*, 8272. [CrossRef]

Disclaimer/Publisher's Note: The statements, opinions and data contained in all publications are solely those of the individual author(s) and contributor(s) and not of MDPI and/or the editor(s). MDPI and/or the editor(s) disclaim responsibility for any injury to people or property resulting from any ideas, methods, instructions or products referred to in the content.